EBioMedicine 60 (2020) 102987

Contents lists available at ScienceDirect

EBioMedicine

journal homepage: www.elsevier.com/locate/ebiom

Research paper

Modulating endothelial adhesion and migration impacts stem cell therapies efficacy

Richard Schäfer[a,b,*], Matthias Schwab[c,d,q,r], Georg Siegel[b], Andreas von Ameln-Mayerhofer[e], Marine Buadze[c], Ali Lourhmati[c], Hans-Peter Wendel[f], Torsten Kluba[g], Marcel A. Krueger[h], Carsten Calaminus[h], Eva Scheer[b], Massimo Dominici[i], Giulia Grisendi[i], Thorsten R. Doeppner[j,k], Jana Schlechter[j], Anne Kathrin Finzel[c], Dominic Gross[c], Roland Klaffschenkel[b], Frank K. Gehring[b,l], Gabriele Spohn[a], Anja Kretschmer[a], Karen Bieback[m], Eva-Maria Krämer-Albers[n], Kerstin Barth[n], Anne Eckert[o], Stefanie Elser[p], Joerg Schmehl[p], Claus D. Claussen[p], Erhard Seifried[a], Dirk M. Hermann[j], Hinnak Northoff[b], Lusine Danielyan[c,q,**]

[a] Institute for Transfusion Medicine and Immunohematology, German Red Cross Blood Donor Service Baden-Württemberg-Hessen gGmbH, Goethe-University Hospital, Frankfurt am Main, Germany
[b] Institute of Clinical and Experimental Transfusion Medicine, University Hospital Tübingen, Tübingen, Germany
[c] Department of Clinical Pharmacology, University Hospital Tübingen, Tübingen, Germany
[d] Dr. Margarete Fischer-Bosch Institute of Clinical Pharmacology, Stuttgart, Germany
[e] Department of Pharmacy, Sindelfingen-Böblingen Medical Center, University of Tübingen, Sindelfingen, Germany
[f] Departments of Thoracic, Cardiac and Vascular Surgery, University Hospital Tübingen, Tübingen, Germany
[g] Departments of Orthopaedic Surgery, University Hospital Tübingen, Tübingen, Germany
[h] Werner Siemens Imaging Center, Department of Preclinical Imaging and Radiopharmacy, University Hospital Tübingen, Tübingen, Germany
[i] Department of Medical and Surgical Sciences for Children & Adults, University Hospital of Modena and Reggio Emilia, Modena, Italy
[j] Department of Neurology, University of Duisburg-Essen, Essen, Germany
[k] Department of Neurology, University Medical Center Göttingen, Göttingen, Germany
[l] 3T GmbH & Co. KG, Tuttlingen, Germany
[m] Institute of Transfusion Medicine and Immunology, German Red Cross Blood Service Baden-Württemberg – Hessen gGmbH, Medical Faculty Mannheim, Heidelberg University, Germany
[n] Institute for Developmental Biology and Neurobiology, Johannes Gutenberg University Mainz, Mainz, Germany
[o] Neurobiology Laboratory for Brain Aging and Mental Health, Molecular and Cognitive Neuroscience, University of Basel, Basel, Switzerland
[p] Department of Radiology, University Hospital Tübingen, Tübingen, Germany
[q] Department of Pharmacy and Biochemistry, University of Tübingen, Tübingen, Germany
[r] Neuroscience Laboratory and Departments of Biochemistry and Clinical Pharmacology, Yerevan State Medical University, Yerevan, Armenia

ARTICLE INFO

Article History:
Received 30 June 2020
Revised 12 August 2020
Accepted 20 August 2020
Available online xxx

Keywords:
Stem cells
Migration
Adhesion
Homing
Stroke
Glioma

ABSTRACT

Background: Limited knowledge of stem cell therapies` mechanisms of action hampers their sustainable implementation into the clinic. Specifically, the interactions of transplanted stem cells with the host vasculature and its implications for their therapeutic efficacy are not elucidated. We tested whether adhesion receptors and chemokine receptors on stem cells can be functionally modulated, and consequently if such modulation may substantially affect therapeutically relevant stem cell interactions with the host endothelium.
Methods: We investigated the effects of cationic molecule polyethylenimine (PEI) treatment with or without nanoparticles on the functions of adhesion receptors and chemokine receptors of human bone marrow-derived Mesenchymal Stem Cells (MSC). Analyses included MSC functions in vitro, as well as homing and therapeutic efficacy in rodent models of central nervous system's pathologies in vivo.
Findings: PEI treatment did not affect viability, immunomodulation or differentiation potential of MSC, but increased the CCR4 expression and functionally blocked their adhesion receptors, thus decreasing their adhesion capacity in vitro. Intravenously applied in a rat model of brain injury, the homing rate of PEI-MSC in the

* Corresponding author at: Institute for Transfusion Medicine and Immunohaematology, German Red Cross Blood Donor Service Baden-Württemberg-Hessen gGmbH, Sandhofstrasse 1, 60528 Frankfurt am Main, Germany.
** Corresponding author at: Department of Clinical Pharmacology, University Hospital Tübingen, Auf der Morgenstelle 8, 72076 Tübingen, Germany.

E-mail addresses: richard.schaefer.md@gmail.com (R. Schäfer), lusine.danielyan@med.uni-tuebingen.de (L. Danielyan).

https://doi.org/10.1016/j.ebiom.2020.102987

brain was highly increased with decreased numbers of adherent PEI-MSC in the lung vasculature. Moreover, in comparison to untreated MSC, PEI-MSC featured increased tumour directed migration in a mouse glioblastoma model, and superior therapeutic efficacy in a murine model of stroke.
Interpretation: Balanced stem cell adhesion and migration in different parts of the vasculature and tissues together with the local microenvironment impacts their therapeutic efficacy.
Funding: Robert Bosch Stiftung, IZEPHA grant, EU grant 7 FP Health

Research in context

Evidence before this study

Despite the first clinical studies reporting on a correlation between the migration potential of transplanted stem cells and their therapeutic efficacy, it is unclear if effective stem cell therapies require reliable and sufficient delivery of the cells to the desired anatomic locations, as well as survival of the cellular graft. Moreover, the many complex processes involved in stem cell interactions with the vasculature, the crucial gatekeeper of their entry into the host's system, have not been elucidated. Specifically, the majority of systemically applied stem cells accumulate as a first pass effect in parenchymal organs such as the liver, spleen and lung increasing the risk of side effects. The mechanisms of this phenomenon are not understood, and it is unclear if and how the re-direction of the transplanted stem cells towards the lesioned tissue would impact the efficacy of a stem cell therapy.

Added value of this study

In this study, by functionally blocking stem cells' adhesion receptors with the cationic linear polymer polyethylenimine, we decreased their adhesion capacity to endothelial cells in vitro and found unexpected differences of chemokine deposits in diseased and healthy rats in the lung vasculature compared to their brains. Together with the reduced endothelial adhesion in the lung, a simultaneous increase of CCR4 expression resulted in chemokine-mediated stem cell homing to lesioned brain tissue and increased migration towards glioblastoma, as well as improved stem cells efficacy in a stroke model. We show that low adhesion to endothelium in healthy tissue and migration to the lesion site are relevant mechanisms for stem cell therapies' efficacy. Our data identify tissue- and organ-specific regulation of stem cell adhesion to and migration through the vasculature, which, together with the local disease specific microenvironment, impact their targeted migration and therapeutic efficacy.

Implications of all the available evidence

Our findings highlight that the reliable and sufficient delivery of a cell therapeutic is critical for its efficacy. The novel concept of modulating adhesion receptor function and chemokine receptor expression by the cationic linear polymer polyethylenimine reported here has the potential to allow highly efficient stem cells homing, hereby contributing to the utilization of their full therapeutic capacity.

1. Introduction

Stem cell therapies hold great promise for a wide variety of diseases including degenerative diseases and cancer [1]. Although their therapeutic mechanisms of action (MoA) involve paracrine effects [2], it is under debate if and to which extend (stem) cell therapeutics require reliable and sufficient delivery to the desired anatomic locations [3,4].

Systemically administered stem cells are recruited to the site of injury by responding to attracting factors [4,5]. However, the majority of the transplanted cells accumulate as a first pass effect in parenchymal organs such as the liver, spleen and lung [4,5]. The mechanisms of this phenomenon are not fully understood, but may involve non-specific trapping of large graft cells in small pulmonary vessels [4,5] in combination with integrin activation [6,7]. Notably, undirected stem cell accumulation in various organs and tissues, as well as vessel obstruction, can increase the risk of side effects. Specifically, vascular embolism by systemically administered stem cells, being widely reported in preclinical studies, can depend on cell dose and infusion velocity of the graft [6,8,9]. Moreover, small vessel entrapment of systemically delivered stem cells reduces their viability, leading to their fragmentation after intravenous (i.v.) infusion [10–12]. Therefore, it is reasonable to assume that the homing capacity of the transplanted stem cells is essential for their therapeutic efficacy, and targeting stem cell delivery is required for dose finding and a prerequisite to unfold their full therapeutic potential.

Due to known interactions between transplanted cells and the host's pulmonary epithelium [5,13–16], different strategies have been developed to optimize stem cell homing. These include increasing the expression of C-X-C chemokine receptor type 4 (CXCR4) [17], or very late antigen-4 (VLA-4) [18], hematopoietic cell E-/L-selectin ligand (HCELL) [19], or P-selectin glycoprotein ligand-1 (PSGL-1) [20] engineering, or a proteolytic modification of the stem cell surface [21]. However, each of the existing approaches addressed only one or a few of the many complex processes involved in the stem cells' interactions with the endothelium, and for nearly a decade no significant progress has been made to clarify the general relevance of such concepts in different disease models of tissue degeneration or cancer.

Addressing this knowledge gap we hypothesized that efficient stem cell delivery to the site of injury would logically require a functional balance of chemokine receptors and adhesion molecules, as well as sufficient trans-endothelial migration. Thus, we developed a novel concept to evaluate the relevance of graft homing as MoA for stem cell therapies, mechanistically focusing on adhesion and migration.

Integrins and VCAM-1 play important roles in adhesion and transmigration [5], and the CD44-hyaluronan and CXCR4-SDF-1 axes play pivotal roles in stem cell trafficking [14,22]. Cations dose-dependently regulate integrin and selectin functions [23–25]. PEI features a high cationic charge density potential, and we hypothesized that it could interact with receptors that mediate stem cell adhesion to EC, resulting in targeted stem cell homing to lesioned tissue hallmarked by high chemokine levels. Therefore, we investigated the applicability of cationic agent PEI treatment to modulate adhesion receptor function. We previously showed that PEI forms complexes with iron nanoparticles (NP) on MSC surfaces before being incorporated by endocytosis [26]. Thus, to assess interactions of PEI-NP complexes with molecules involved in MSC adhesion and migration, we also tested the combined formulation of PEI with NP.

Hereby, our study highlights the relevance of stem cells' homing for their therapeutic efficacy.

2. Methods

2.1. Overview of in vitro and in vivo studies

The concept of the study was to investigate the relevance of adhesion and migration of transplanted MSC for their therapeutic efficacy. Thus, we treated the MSC with either PEI or with PEI-NP to study the impact on expression and function of their adhesion and chemokine receptors in vitro. The results were then further validated in vivo focusing on the endpoints of first-passage filtering in the lung, targeted homing and migration to lesioned tissue, as well as therapeutic potential.

In our in vitro and in vivo studies, we investigated human BM-MSC that were collected from at least 10 individual donors of both genders. After basic characterization of the MSC, we assessed the detectability of chemokine and adhesion receptors on their surface by flow cytometry and the respective mRNA expression of these genes after treatment with PEI or with PEI-NP. For selected targets we additionally quantified their intra- and extracellular presence by ELISA. Receptors that could not be detected were not further analysed. Additionally, PEI/PEI-NP treatment effects on MSC functions such as differentiation, immunomodulation and trophic factor production were investigated in vitro. Next, we explored the impact of PEI/PEI-NP-mediated receptor modulation on MSC adhesion and migration in vitro including specific receptor blocking.

As this allowed us to modulate MSC adhesion and migration in vitro, we next tested the functional blockade of adhesion receptors together with increased chemokine receptor expression of MSC in vivo. Specifically, we addressed the first-pass effect of PEI-treated and untreated MSC in the lung and targeted homing in a rat quinolinic acid (QA) brain lesion model and the tissue migration of MSC in a mouse glioblastoma model. To better understand, whether and to which extent the migration of exogenously applied stem cells may be intrinsically predetermined by the organ-specific chemokine milieu in health and disease, brain and lung chemokines were quantified in healthy, QA-lesioned and spontaneously hypertensive stroke prone rats (SHRSP). Finally, we evaluated the therapeutic effects of PEI-treated and untreated MSC in a murine stroke model.

2.2. Ethics statements

Human BM was obtained after informed consent and its use was approved by the institutional review boards (ethical committees) of the Universities of Tübingen (reference number 76/2009BO2) and Frankfurt (reference number 329/10).

All animal experiments were carried out in accordance with institutional animal welfare guidelines and approved by the local institutional committee of Animal Welfare in Tübingen and Duisburg-Essen.

2.3. Primary cells, cell lines and cell cultures

BM was taken under sterile conditions from donors after informed written consent during orthopedic operations: From each donor 5-10 mL of whole BM was collected in a sterile syringe.

To isolate human MSC from whole BM we used the technology as described previously [27]. Briefly, BM mononuclear cells were isolated by density gradient centrifugation on Lymphoflot (Biotest, Dreieich, Germany), washed twice with PBS (Lonza, Walkersville, U.S.A.), counted and seeded at a density of 1×10^5 cells per cm^2 in medium composed of α-MEM (Lonza), 1% penicillin-streptomycin (PS; Lonza) and 10% fetal calf serum (FCS; Lonza, Switzerland) or 10% human AB serum (ZKT, Tübingen, Germany) to tissue culture flasks (Nunc, Roskilde, Denmark). The resulting passage (P) 0 cultures were kept at 37 °C in humidified atmosphere with 5% CO_2. Non-adherent cells were removed by washing after 24 h and medium was changed twice a week. Subconfluent MSC were detached using Trypsin-EDTA (Lonza), counted using a CASY® cell counter (Roche, Basel, Switzerland) and plated to fresh tissue culture flasks for the next passage (P1) at a density of 1,000 cells per cm^2.

Primary human aortic endothelial cells (hAoEC) and primary human pulmonary microvascular endothelial cells (hpMEC) were purchased from Promocell, Heidelberg, Germany. Primary human brain microvascular endothelial cells (hbMVEC) were purchased from Pelo Biotech GmbH, Planegg, Germany.

2.4. Transduction of human BM-MSC with green fluorescent protein (GFP)

Human eGFP+ BM-MSC were generated by the eGFP-encoding bicistronic murine stem cell virus derived retroviral vector (pMIGR1) system as described previously [28,29] or by the Mission TurboGFP™ lentiviral particles system (Sigma-Aldrich).

2.5. U87MG-DsRed-Virus production and Transfection of U87MG cells

A lentivirus was engineered from lentiviral backbone plasmid pPRIME-mating recipient plasmid with CMV promoter controlling dsRed expression by transfecting HEK 293T cells with a mix of 15 μg of pPRIME-CMV-dsRed-recipient, 10 μg of packaging plasmid (pSPAX2) and 6 μg of coat plasmid (pMD2G) [30]. The pPRIME-CMV-dsRed-recipient was a gift from S. Elledge (Addgene plasmid # 11658) [31]. The virus-containing medium was harvested and pooled during two days. The virus was then concentrated 10-fold by ultracentrifugation (80,000 x g at 4 °C for 90 min) and used for infection.

On the day of infection, medium was removed and 1 mL of virus 10x supplemented with protamine sulphate (8 μg/mL) was applied to the U87MG cells drop by drop. After 3 days, the medium was exchanged with fresh culture medium to amplify the cells. A flow cytometry with fluorescence activated cell sorting (FACS) was performed to separate the DsRed positive cells from the non-infected cells based on fluorescent labelling. The sorted DsRed-positive U87MG cells were re-plated and amplified until usage.

2.6. Treatment of human BM-MSC with polyethylenimine alone or in combination with iron nanoparticles

Human BM-MSC treatment was performed at 90% confluency for 4 h in T-75 flasks. One day before treatment, cell culture media were changed and reduced to 9 mL per flask. The next day, MSC were treated for 4 h with the cationic linear polyethylenimine jetPEI™ (PolyPlus Transfection, Illkirch, France) at a final concentration of 10 μL/mL (PEI-MSC), or with a formulation of 10 μL/mL jetPEI™ plus 60 μg/mL Ferucarbotran (Resovist®, Bayer Schering AG, Berlin, Germany) consisting of superparamagnetic iron oxide nanoparticles (mean particle diameter 4–6 nm) coated with carboxydextran (mean hydrodynamic diameter 60 nm) as described previously (PEI-NP-MSC) [26]. During the treatment the cells were kept in the incubator (37 °C, 5% humidified CO_2). After the treatment the cells were washed with PBS and cultivated for 24 h in 15 mL culture medium before the harvest and processing for in vitro assays or in vivo transplantation.

2.7. In vitro MSC differentiation assays

MSC can be functionally characterised by their in vitro differentiation capacity, and we evaluated the differentiation potential into the adipogenic, osteogenic and chondrogenic lineage as described previously [27]. Briefly, for adipogenic and osteogenic differentiation MSC were seeded at a density of 1000 cells per cm^2 and kept under standard culture conditions until reaching subconfluency. Subsequently, either adipogenic differentiation was induced using the hMSC Adipogenic BulletKit (Lonza), or osteogenic differentiation was induced using “osteogenic medium” composed of α-MEM (Lonza), 1% PS

(Lonza), 10% FCS, 10^{-8} M dexamethasone, 0.2 mM ascorbic acid and 10 mM β-glycerolphosphate (Sigma-Aldrich). After three weeks under differentiation conditions, lipid vacuoles in adipogenic cultures were stained with Oil Red O and calcium deposits of osteogenic cultures with Alizarin Red S, respectively. For chondrogenic differentiation, 2.5×10^5 MSC were kept in micromass pellet cultures. Differentiation was induced using the hMSC Chondrogenic Differentiation BulletKit (Lonza), supplemented with TGF-β 3 (Lonza) as a growth factor. After four weeks of differentiation, frozen sections of fixed pellets were performed and stained with Alcian blue.

2.8. Flow cytometry analyses

To assess the characteristic surface epitope pattern of human BM-MSC, flow cytometry analysis of surface marker expression was performed with a FACScan (BD Biosciences, Heidelberg, Germany) using BD CellQuest Pro™ software and the following antibodies: anti-CD10, -CD14, -CD15,-CD19, -CD29, -CD31, -CD34, -CD43, -CD44, -CD45, -CD56, -CD59, -CD71, -CD73, -CD90, -CD105, -CD106, -CD117, -CD130, -CD140a, -CD140b, -CD146, -CD166, -GD2, -HLA class I and -HLA class II (BD Biosciences); -CD93 (R&D Systems, Minneapolis, U.S.A.); -CD133 and -CD271 (Miltenyi Biotec, Bergisch-Gladbach, Germany); -CD243 (Millipore); -CD173 (AbD Serotec, Puchheim, Germany) and -W8B2 (BioLegend, San Diego, U.S.A.). Podoplanin (PDPN) expression was analysed with rat anti-human-podoplanin antibody (BioLegend). PE-conjugated or non-labeled IgG1, -IgG2a and -IgM antibodies (BD Biosciences) were used as isotype matched controls. Secondary antibody was a polyclonal PE-conjugated goat anti-mouse Ig (BD Biosciences).

Flow cytometry analysis for the evaluation of the homing receptors on the cellular surface of MSCs was performed with FACSort flow cytometer (BD Biosciences) using BD CellQuest Pro™ software. The cells were detached with Accutase™ (GE Healthcare) 24 h after treatment, washed and re-suspended in FACS buffer (PBS + 0.1% FCS). Each sample contained a cell suspension with 2×10^5 cells in 100 μL FACS buffer. Staining was performed according to the manufacturer`s instructions with FITC- or PE-conjugated antibody and incubated for 30 min in the dark, followed by two washing steps. The following antibodies were used to investigate the expression of cell adhesion receptors and chemokine receptors on untreated MSC: Anti-human-α-1integrin (CD49a/VLA-1), -α-4integrin (CD49d/VLA-4), -β-1integrin (CD29), -H-CAM (CD44), -P-Selectin/LECAM-3 (CD62P), -endoglin (CD105), -VCAM (CD106), -CCR1 (CD191), -CCR4 (CD194), -CCR5 (CD195), -CCR6 (CD196), -CCR7 (CD197), -CXCR4 (CD184), -CXCR5 (CD185), -CXCR6 (CDw186/BONZO), and -CCR9 (CDw199). The following antigens that were found to be expressed on untreated MSC were used to further analyse MSC treated with PEI alone or in combination with nanoparticles: Anti-human-α-1integrin (CD49a/VLA-1), -α-4integrin (CD49d/VLA-4), -β-1integrin (CD29/VLA-4), -H-CAM (CD44), -P-Selectin/LECAM-3 (CD62P), -endoglin (CD105), -VCAM (CD106), -CCR4 (CD194), -CXCR4 (CD184), and -CCR9 (CDw199). For details of fluorescence conjugation, immunoglobulin subtype/isotype and vendors see Table 1 below. For analysis, the geometric mean of the fluorescence intensity was used. To compare to antigen expression on treated and untreated MSC, the antigen expression on untreated MSC was set at 100%. Data were analysed as relative values according to the respective untreated MSCs of the same MSC preparation (donor). To analyse PEI dose-dependent CCR4 expression human BM-MSC were treated with different PEI doses (1.0%, 0.5% and 0.25%), and CCR4 staining was performed as described above.

2.9. Determination of cell viability and diameter

Cellular viability and diameter of detached cells was examined with the CASY®2 Cell Counter and Analyzer System, Model TT (Roche Diagnostics, Mannheim, Germany) according to the ECE method described by Lindl et al. [32].

Table 1
Antibodies used for flow cytometry analysis of homing receptors on human BM-MSC:

Specificity	Fluorochrome	Immunoglobulin subtype/isotype	Vendor
CD29	FITC	IgG_1	Serotec
CD44	FITC	IgG_1	R&D
CD49a	PE	IgG_1	BD Biosciences
CD49d	PE	IgG_1	R&D
CD49e	PE	IgG_1	R&D
CD62P	FITC	IgG_1	R&D
CD105	FITC	IgG_1	R&D
CD106	FITC	IgG_{2a}	R&D
CCR1	FITC	IgG_{2b}	R&D
CCR4	PE	IgG_{2b}	R&D
CCR5	PE	IgG_{2b}	R&D
CCR6	PE	IgG_{2b}	R&D
CCR7	FITC	IgG_{2a}	R&D
CCR9	PE	IgG_{2a}	R&D
CXCR4	FITC	IgG_{2a}	R&D
CXCR5	PE	IgG_{2b}	R&D
CXCR6	PE	IgG_{2b}	R&D

2.10. In vitro migration assays

Human BM-MSC in vitro migration capacities were analysed using a 6-well transwell chamber system (Polyethylene Terephthalate membrane; pore size: 8 μm [Corning, Treyburn, NC, U.S.A]).

Migration medium (α-MEM + 10% human platelet lysate [HPL] + 1%PS + 2IU heparin/mL) without or with cytokines (25 ng/mL PDGF-BB, or 200 ng/mL CCL2 all from Peprotech, Rocky Hill, NJ, U.S.A.) was added to the lower compartment. Then untreated or PEI-treated human BM-MSC (2.8×10^5 cells per well) in migration medium without cytokines were placed into the upper compartments. After 24 h migration time cells and medium from the upper compartments were discarded. To harvest all transmigrated cells the medium of the lower compartments was collected and possibly adherent cells were detached from the lower side of the membrane and the surface of the well by incubation with Accutase™ (Gibco) at +37 °C. After 5 min the enzyme activity was antagonized with complete medium and the lower side of the membrane and the well were rinsed thoroughly, and the detached cells´ suspension was added to the migration medium from the lower compartment. Subsequently, transmigrated hBM-MSC were lysed and quantified by CellTox™ Green Cytotoxicity Assay (Promega, Madison, WI, USA).

To investigate the migration capacity of human BM-MSC subpopulations the above described 6-well transwell chamber system was used. First, migration medium (α-MEM + 20% pooled human serum [IKET, Tübingen, Germany] + 1%PS) without or with cytokines (50 ng/mL CCL2 or 20 ng/mL CXCL12, both from Peprotech) was added to the lower compartment. Then untreated or PEI-treated pooled (6 donors) human BM-MSC (2.8×10^5 cells per well) in migration medium without cytokines were placed into the upper compartments. Additionally, untreated or PEI-treated pooled (6 donors) human BM-MSC were seeded in 6 well plates without transwell inserts as reference group. After 24 h the cells were harvested as described above and analysed, using 7AAD dead cell exclusion staining, by flow cytometry. Human BM-MSC subpopulations were identified by labelling with anti-CD10 (BD Biosciences), anti-CD140b (BD Biosciences), anti-CCR4 (R&D), or anti-GD2 (BD Biosciences). Migration capacities of human BM-MSC subpopulations were assessed by analyses of percent of migrated antigen positive cells normalized to percent antigen positive cells of the respective reference groups.

2.11. Small EV isolation and nanoparticle tracking analysis

Supernatants of treated or untreated human BM-MSC were collected and subjected to differential centrifugation (all steps at 4 °C): 10 min at 130 x g to clear supernatants from cell debris, followed by 30 min at 10,000 x g to pellet microvesicles (MVs), and ultracentrifugation for 2 h at 100,000 x g to pellet small EV. The final 100,000 x g pellet was re-suspended in PBS and analysed using the Nanosight LM10 system at 23 °C (green laser 532 nm, syringe pump, Nanosight 2.3 software). The following settings were used: Camera level =16, particle detection with a screen gain of 16, a detection threshold of 7 and the setting "minimum expected particle size auto". A script control was used (repeat start, syringe load 500, delay 5, syringe stop, delay 15, capture 30, repeat 4). Per sample five 30 s videos were recorded, the particles were tracked and average values were calculated to express particle number over size.

2.12. Immunocytochemistry and immunohistochemistry

For the immunofluorescence staining of CXCR4 in vitro, human BM-MSC were cultured and treated with PEI or PEI-NP in chamber slides (Becton Dickinson). Cell samples were incubated with the primary antibody against CXCR4 or an isotype control (both IgG2B, R&D), 1:25, followed by incubation with the secondary fluorochrome-labelled antibody (Alexa Fluor 488, Invitrogen) 1:300, for 30 min at 37 °C each. Samples were embedded in mounting medium containing DAPI and documented with a fluorescence microscope (Zeiss) and the AxioVision Rel. 4.8 software (Zeiss).

Brain and lung sections of QA-lesioned rats, selected from the vicinity of the sections containing human eGFP+BM-MSC, were fixed with methanol at −20 °C, washed and subsequently incubated with antibodies against von Willebrand factor (vWF) diluted 1:300 (rabbit polyclonal, DakoCytomation, Glostrup, Denmark), or SDF-1 diluted 1:50 (rabbit polyclonal, Abcam), or CCL2 diluted 1:200 (rabbit polyclonal, Biozol, Eching, Germany) for 2 h at room temperature (RT). Brain sections were also stained with CXCR4 antibodies, diluted 1:300 (R&D) for 2 h at RT. Sections were washed with PBS and further incubated with Cy3-conjugated goat anti-rabbit IgG diluted 1:500 (Dianova, Hamburg, Germany) for 1 h at RT. Thereafter, samples were washed with 0.05% Triton (Sigma-Aldrich) in PBS, coated with Vectashield mounting medium containing DAPI and assessed by fluorescence microscopy.

Immunohistochemical analyses of brain sections from mice with focal cerebral ischemia were performed as described before [33]. Briefly, 16-μm thick coronal cryostat sections were obtained after sacrifice of animals and subsequent transcardial perfusion with both PBS and 4% paraformaldehyde. Quantitative analysis was performed in four regions of interest (ROI) within the ischemic basal ganglia, i.e., at 0.14 mm anterior, 2.5−3.25 mm ventral, and 1.5−2.25 mm lateral from bregma. Three sections per animal and ROI were used.

Brain sections were stained with polyclonal rabbit anti-GFP antibody (1:2,500; Abcam, U.K.), goat anti-doublecortin antibody (1:50; Santa Cruz Biotechnology), polyclonal rat anti-GFAP antibody (1:500; Zymed, Germany), monoclonal mouse anti-CNPase antibody (1:400; Millipore, U.K.), monoclonal mouse anti-NeuN antibody (1:1,000; Millipore) and monoclonal mouse anti-nestin antibody (1:500; Millipore). Sections were then incubated with goat anti-mouse Cy-3 (1:100; Jackson ImmunoResearch, U.K.), goat anti-rat Cy-3 antibody (1:200, Abcam), and donkey anti-goat Cy-3 secondary antibody (1:500; Dianova) respectively.

2.13. Immune cell proliferation assays

The immunosuppressive properties of PEI/NP treated and untreated human BM-MSC were analysed in co-culture assays with activated allogeneic immune cells. Four PEI/NP treated and untreated human BM-MSC preparations were mitotically inactivated by treatment with 40 μg/mL mitomycin c for 30 min at 37 °C in serum free medium. Thereafter, the MSC were washed three times, counted and seeded to 96-well plates in triplicates at a density of 2×10^4 cells per well. After 24 h, 1×10^5 peripheral blood mononuclear cells (PBMNC), freshly isolated by density-gradient centrifugation from heparinized blood of 2 unrelated healthy donors, were added to the respective wells of BM-MSC cultures. Immune cells were stimulated with 10 μg/mL phytohaemagglutinin-L (Sigma-Aldrich) and cultured for 72 h under standard culture conditions. During the last six hours, 100 μM bromodeoxyuridine (BrdU) labelling solution from the Cell Proliferation ELISA, BrdU (colorimetric) Kit (Roche) was added to the (co-) cultures and cell proliferation was assessed by ELISA, using the anti-BrdU antibody provided in the kit according to the manufacturer's instructions. Photometric light absorption was measured in a plate reader and absorbance values were averaged and normalized to the PBMNC only control of the respective blood donor.

2.14. RNA isolation and qRT-PCR analyses

RNA from PEI-MSC, PEI-NP-MSC, as well as from untreated MSC from 10 unrelated donors was isolated using the RNeasy Mini Kit (Qiagen, Hilden, Germany) according to the manufacturer's instructions. Remaining genomic DNA was digested using the RNase-Free DNase Set (Qiagen). RNA concentration was assessed using a NanoDrop photometer (ThermoFisher Scientific). RNA was stored at −80 °C for up to three months. For analysis by quantitative PCR, 0.5 μg RNA (samples for *CXCR4* mRNA and *H-CAM* mRNA) or 1 μg RNA (samples for *endoglin* mRNA, *VCAM-1* mRNA, *integrin α 1* mRNA, and *CCR4* mRNA) from each sample was reverse transcribed using the Transcriptor First Strand cDNA Synthesis Kit (Roche) or the Tetro cDNA Synthesis Kit (Bioline, Luckenwalde, Germany) according to the manufacturer's instructions. Resulting cDNA was stored at -20 °C for up to 6 months. For expression analysis of *CXCR4* mRNA, *H-CAM* mRNA, *endoglin* mRNA, *VCAM-1* mRNA, *integrin α 1* mRNA, *CCR4* mRNA and *GAPDH* mRNA as housekeeping gene, PCR analysis of cDNA was performed using ready-to-use amplification primer mixes for RT-PCR (search-LC, Heidelberg, Germany) in combination with LightCycler FastStart DNA Master SYBR Green I (Roche) and the LightCycler Instrument (Roche), according to the manufacturer's instructions. PCR results were analysed by normalizing the expression of each target gene to the expression of the housekeeping gene *GAPDH* in each sample.

2.15. Protein isolation and Western blot analyses

Western blotting was performed using protein lysates from PEI/NP-treated or untreated human MSC and from brain homogenates of unilaterally QA-lesioned rats. The total protein was determined by DC Protein assay (Bio-Rad). For each lane, 50 μg of protein were subjected to sodium dodecyl sulphate polyacrylamide gel electrophoresis in a 12.5% or 10% gel and transferred to PVDF membranes by tank blotting. Membranes were blocked in 0.66% (v/w) I-Block or 5% w/v nonfat dry milk (Tropix, Applied Biosystems, Weiterstadt, Germany) in PBST or TBST (0.05% Tween 20 in PBS or TBS, with pH 7.4) for 1.5 h. Antibodies against CXCR4 (1:500, AbD Serotec), CD44 (1:1000, Cell Signaling Technology, Danvers MA, USA), CCL-2 (1:500, Biozol), and GAPDH (1:1000, loading control, Millipore) were used.

2.16. ELISA, Luminex® and V-plex® assays

In order to investigate whether the treatment of MSC with PEI +/-NP could split off the soluble fraction from the CD44 molecule hereby altering the function of CD44, we quantified CD44 protein in the supernatants of untreated and treated human BM-MSC by Human

sCD44std Instant ELISA according to the instructions of the manufacturer (Bender MedSystems, Vienna, Austria).

The capacity to produce and secrete trophic factors that have been shown to mediate therapeutic effects of MSC was assessed in supernatants and lysates of untreated and treated human BM-MSC. Pooled human BM-MSC (8 donors) were seeded at P2 into 12-well plates in biological triplicates at a density of 20,000 cells/cm^2. After 24 h, cells were treated with PEI or PEI+NP, or kept in standard culture medium as untreated control. During the treatment the cells were kept in the incubator (37 °C, 5% humidified CO_2 atmosphere). Thereafter, treated and untreated cells were washed with PBS and cultivated under standard culture conditions for another 24 h. Culture supernatants were transferred to Eppendorf vials and frozen at −80 °C for following analysis. Cell monolayers were washed with ice cold PBS, lysed in 400 μL Procarta® lysis buffer (Affymetrix) and frozen at −80 °C. Samples were sent to Multimetrix (Heidelberg, Germany) for multiplex analysis of expression of HGF, LIF, VEGF-A, FGFb and NGF-b in a commercial Luminex® system. For analysis of BMP4 and angiopoietin-1 expression, samples were analysed using Quantikine® ELISA systems (R&D) according to the manufacturer's instructions. All samples were analysed in technical duplicates.

For analyses of cytokines, the brains and lungs of QA-lesioned, SHRSP and normal Sprague-Dawley rats (Charles River) were processed in ice-cold lysis buffer (300 mmol/L NaCl, 50 mmol/L Tris, 2 mmol/L $MgCl_2$, 0,5% Nonidet™ P40, containing a Complete Protease Inhibitor Tablet from Roche Diagnostics at a ratio of 1:5 (tissue weight/buffer volume). The tissue was disrupted using a Micro Dismembrator II (B.Braun, Melsungen, Germany) at maximal amplitude for 30 s in a Teflon container which had been precooled with liquid nitrogen. Thereafter, homogenates were clarified by centrifugation at 20,000 x g and 4 °C for 15 min. Determination of rat cytokines (monocyte chemotactic protein [MCP]-1, interferon [IFN]-γ, tumor necrosis factor [TNF]-α, regulated and normal T cell expressed and secreted [RANTES], interleukin [IL]-1α,IL-1β, IL-6, IFN-γ-induced protein [IP]-10 [CXCL10], MCP-3, and macrophage inflammatory protein [MIP]-1α) was performed using a multiplex bead immunoassay system (Procarta® Cytokine Assay Kit; Affymetrix, Inc., Santa Clara, CA, U.S.A.) according to the manufacturer's manual. The results are presented as pg/mL or pg/mg protein.

For quantification of pro-migratory cytokines primary endothelial cells derived from human brain (hbMVEC) and from human lung (hpMEC) were treated with lysis buffer (300 mM NaCl, 50 nM Tris, 2 mM $MgCl_2$, 0.05% NP40) and, after centrifugation (20,000 x g and 4 °C for 15 min), supernatants were harvested.

Total protein concentrations in the supernatants were quantified with BCA protein assay (ThermoFisher Scientific). Determination of the human pro-migratory cytokines CCL2, PDGF-BB and TGF-β was performed using respective ELISA kits (CCL2 and PDGF-BB: Cloud Clone [Katy, Tx, USA]; TGF-β: Biorbyt [Cambridge, UK]) according to the manufacturer's manual. The results are presented as pg/μg total protein.

2.17. Flow chamber assays

HAoEC (Promocell) were seeded into ibidi microslides (μ-Slide I (0.4) Luer, Collagen IV, IBIDI, Munich) at a density of 7.2 × 10^5 cells/cm^2 and incubated overnight, resulting in a confluent adherent layer. HAoECs were then activated with 2.5 ng/mL TNFα (R&D, Wiesbaden, Germany) for 16 h at 37 °C.

Treated or untreated human BM-MSC from 2 to 5 unrelated donors (P4 or P5) were washed, detached with trypsin, counted and adjusted at a concentration of 3 × 10^5 cells/mL. The microslides were incorporated into a flow-based adhesion assay. Briefly, a syringe pump (PHD 2000, Harvard Apparatus, Natick, MA, U.S.A.) moved the cell suspension in medium through the microslides at a controlled rate of 0.1 mL/min, while allowing visualisation of the cells inside the slide by phase contrast microscopy (Axiovert, Zeiss, Oberkochen, Germany). MSC were perfused through the microslides for 10 min. For analysis of MSC adhesion under shear stress conditions, video sequences (10 s) were recorded by a digital camera (CF15 MC, Kappa, Gleichen, Germany). A cell moving less than one cell diameter within 10 s. was defined to be adherent. To measure velocities, images from these video sequences were digitalized at 25 frames/s, and the distance of movement of the MSC during the 10 s. interval was computed into pixels. All measurements were performed using customized software for image recognition as described previously (CellTracker, C. Zanke, University Hospital Tübingen, Germany) [34].

To evaluate the influence of surface antigens on adhesion, we conducted blocking experiments with appropriate antibodies. PEI/NP and untreated human BM-MSC were incubated with 10 μg/mL anti-CD44 antibodies (BD, Heidelberg, Germany) or anti-CXCR4 antibodies (R&D Systems) for 30 min. Chinese Hamster Ovary Cells (CHO-A5) were used as negative controls.

2.18. Dynamic adhesion capacity of human BM-MSC in vitro

To analyse PEI treatment effects on adhesion over time, human BM-MSC were treated with PEI or mock-treated as described. Then 1 × 10^4 cells were seeded per well of an 8-chamber slide (Nunc) in culture medium, 10% FCS. Adhesion was monitored using kinetic live cell imaging (IncuCyte Zoom, Essen Biotech) in 2-min intervals for 30 min. Phase object area and % confluence were calculated. Integrin signalling was monitored in parallel chamber slides assessing phosphorylation of focal adhesion kinase (FAK) and paxillin (PAX) as described before [35]. The following antibodies were used: pFAK: mouse monoclonal IgG1, clone 2D11, 1:50, Santa Cruz; FAK: rabbit polyclonal IgG, clone C-20, 1:50 (Santa Cruz); pPax: mouse monoclonal IgG1, clone 2D11, 1:50,Santa Cruz; Pax: mouse monoclonal IgG1, clone 2D11, 1:50 (Santa Cruz).

2.19. Quartz Crystal Microbalance with Dissipation (QCM-D) experiments

All QCM-D experiments were performed using a qCell T instrument (3T analytik, Tuttlingen, Germany) and 10 MHz gold coated quartz sensor chips at a temperature of 37.2 °C. Before each measurement, the QCM-D setup (i.e., tubes, junctions, crystals and flow chamber) was cleaned with 1% sodium hypochlorite at a flow rate of 100 μL/min for 30 min, and rinsed with Ampuwa® (Fresenius Kabi, Germany) at a flow rate of 800 μL/min for 22 min and culture media (HEPES-buffered alpha-MEM consisting of 379.05 mL Ampuwa, 50 mL MEM (10x), 12.5 mL HEPES (1M), 3.45 mL Glutamine (200 mmol), 50 mL human AB serum, 5 mL PS) at a flow rate of 60 μL/min for 3 min, followed by a flow rate of 800 μL/min for 1 min. Cells, with or without PEI/NP treatment or heat treatment (negative control; 10 min. 57 °C; dead cells), suspended in culture media at a concentration of 1.3 million cells/mL (corresponding to about 40,000 cells in the flow chamber with a volume of 30 μL), were then seeded at stagnant conditions throughout the 4 h measurements. After each measurement, the cells were crystal violet stained (according to manufacturer's instructions) and viewed by microscopy (Axioskop 2MAT, Zeiss). Each condition was carried out in triplicate.

2.20. Animal models and SC transplantations

For all in vivo transplantation experiments human eGFP+ BM-MSC were used.

2.21. Human orthotopic brain tumour model and human BM-MSC implantation

Stereotactic brain injection of human glioblastoma U87MG-DsRed cells (1×10^5 cells in 2 μL of sterile PBS) was performed in 9-weeks old female NMRI mice (Charles River Laboratories). 22 days after tumor inoculation 1×10^5 eGFP+ PEI-treated and eGFP+ untreated human MSC ($N = 4$ per group) or PBS ($N = 3$) were injected contralaterally to the following coordinates relative to bregma: DV −3.0; AP +1.0; ML −1.5. Both glioblastoma and MSC were injected in a total injection volume of 2 μL with a 26 gauge needle (Hamilton, Bonaduz, Switzerland) at a flow rate of 1 μL/min. Anesthesia was performed using a mixture of medetomidine (0.5 mg/kg), midazolam (5.0 mg/kg) and fentanyl (0.05 mg/kg) and was abrogated with flumazenil (0.5 mg/kg) and atipamezole (2.5 mg/kg). Six days after injection of PEI-treated and untreated human MSC animals were euthanised with CO_2.

2.22. MR imaging

MR scans were acquired using a 7T ClinScan MR-Scanner (Bruker, Ettlingen, Germany) eighteen days after implantation of glioblastoma U87MG-DsRed cells. Animals were anesthetized with a mixture of 1.5% isoflurane (Abbott, Wiesbaden, Germany) evaporated in oxygen at a flow of 0.5 L/min . A dedicated brain coil was used to obtain T2-weighted images of the brain. For the maintenance of the body temperature at 37 °C a heating system connected to a rectal temperature sensor was employed. Image analysis was performed by Inveon Research Workplace 3.1 (Siemens Preclinical Solutions, Erlangen, Germany)

2.23. Excitotoxic quinolinic acid brain injury and human BM-MSC transplantation

Male Sprague-Dawley rats (Charles River, weight at start of experiments: 220–300 *g*, age 9–11 weeks) were held under constant climatic conditions in an animal holding room with 12:12 h light-dark cycle. All experiments were performed in the light phase. The rats had access to 15 g standard rat chow per day and water *ad libitum*.

For unilateral lesion of the hippocampus, the animals were anaesthetized either with pentobarbital (64 mg/kg) or isoflurane (1–2%) in air with perioperative fentanyl anaesthesia (3–5 μg/kg *s.c.*). Post-surgery analgesia treatment was performed by carprofen injections (daily 50 mg/kg *s.c.*). The head of each animal was fixed in a stereotactic frame (Stoelting, Dublin, Ireland), the skin above the skull was treated with iodine solution for disinfection, and a short incision was made through the skin. Small holes were drilled at the distinct stereotactic localization for the hippocampus without injury of the dura mater. The quinolinic acid (QA, Sigma-Aldrich) microinjection (60 mmol/μL) was performed by means of a Hamilton microsyringe (cannula diameter 0.45 mm) over one minute into the left hippocampus (coordinates relative to bregma: AP −3.8 mm, L +2.4 mm, V −3.2 mm). The cannula was left in place for another two minutes and was slowly retracted afterwards. The skull holes were carefully closed by means of bone wax and the skin was closed using 2–4 sutures. In all rats the wound healed without complication within 2 −3 days after surgery.

Untreated, PEI or PEI-NP treated human eGFP+ MSC (5×10^6 cells) were re-suspended in 800 μl sterile phosphate buffered saline and were administered 7 days after surgery by intravenous injection into the lateral tail vein under a short ketamine-anaesthesia (100–125 mg/kg *i.p.*). The numbers of animals per group were: 5 (untreated MSC; immunohistochemistry), 5 (PEI-MSC; immunohistochemistry); 6 (PEI-NP-MSC; immunohistochemistry); 12 (no cells; 6 with lesion, 6 without lesion; multiplex).

The preparation of the tissue was performed 24 h after cell administration after decapitation of the respective animal using a guillotine under ketamine anaesthesia. Left and right lung and both brain hemispheres were removed and frozen for immunohistochemical and multiplex analyses as described above.

Sagittal cryosections (20 μm in thickness) were prepared from the left and right brain hemispheres of rats. For detection of the human eGFP+ MSC, the sections were stained with 4′,6 diamidino-2-phenylindole (DAPI) (Vector Laboratories Burlingame, CA, USA). For MSC quantification, sagittal sections were taken at regular intervals starting from inter-hemispheric fissure and analysed by fluorescence microscopy using an Olympus BX51 microscope (Olympus) and the "AnalySIS" software (Soft Imaging System GmbH, Germany). The numbers of eGFP+ MSC were obtained from the areas of interest (hippocampus, lateral ventricle, striatum) and in total per brain section. The data shown in Fig. 5 show the number of cells per μm^2 quantified from 50 sections per brain.

Longitudinal cryosections (25 μm in thickness) of the whole left lung were taken at regular intervals and either mounted with DAPI for MSC quantification or processed for immunocytochemistry as described above. MSC quantification was performed from 5 fields per lung section (30 sections per organ).

2.24. Spontaneously hypertensive stroke prone rats

Male 7 weeks-old spontaneously hypertensive stroke prone (SHRSP) rats purchased from Charles River were kept in groups of 3 or 4 animals under standardized conditions (air humidity: 60%; Temp: 22 °C; darkness from 7 pm to 7 am) and given salt-rich (2%) chow (Altromin, Lage, Germany) and 1% NaCl drinking water solution *ad libitum*.

After 12 weeks of salt loaded diet, animals were sacrificed under ketamine anaesthesia (100 mg/kg, *i.p.*; Delta Select, Pfullingen, Germany). The brains and lungs were isolated and stored at −80 °C for further analyses by immunohistochemistry, Western blots and Luminex assay as described above.

2.25. Induction of focal cerebral ischemia and transplantation of human BM-MSC

All mice had free access to food and water, and all experiments were blinded to experimenters. Adult male C57BL6 mice (Harlan, Germany; 10 weeks old, 25 *g*) were exposed to 45 min. of transient focal cerebral ischemia using the thread occlusion model as previously described [36,37]. Briefly, mice were anesthetized using a volatile mixture consisting of isoflurane (1.5%), nitrogen (78.5%) and oxygen (30%). Under constant Laser Doppler control of regional blood flow, a silicon-coated filament (180 μm in diameter; Doccol, USA) was inserted into the left common carotid artery and gently pushed upwards into the left middle cerebral artery (MCA). The filament was withdrawn after 45 min. and regional blood flow was controlled for an additional 10 min. to ensure proper reperfusion. Subsequently, 1×10^6 MSC or PEI-MSC were administered into the femoral vein. Cells were re-suspended in 200 μL PBS and control animals received 200 μL PBS only, $N = 7$ animals per group.

2.26. Behavioural tests

2.26.1. Rotarod, tight rope, corner turn test

For assessment of functional impairment, three well established behavioural tests were used on days 10, 20 and 28 post-stroke [36]. Before performance of actual tests at the aforementioned days, mice were trained 1–2 days before stroke induction in order to ensure proper test performance of animals. The rotarod test was performed using a treadmill with a diameter of 3 cm (TSE Systems, Germany). The test was performed using accelerating velocity (4–40 rpm),

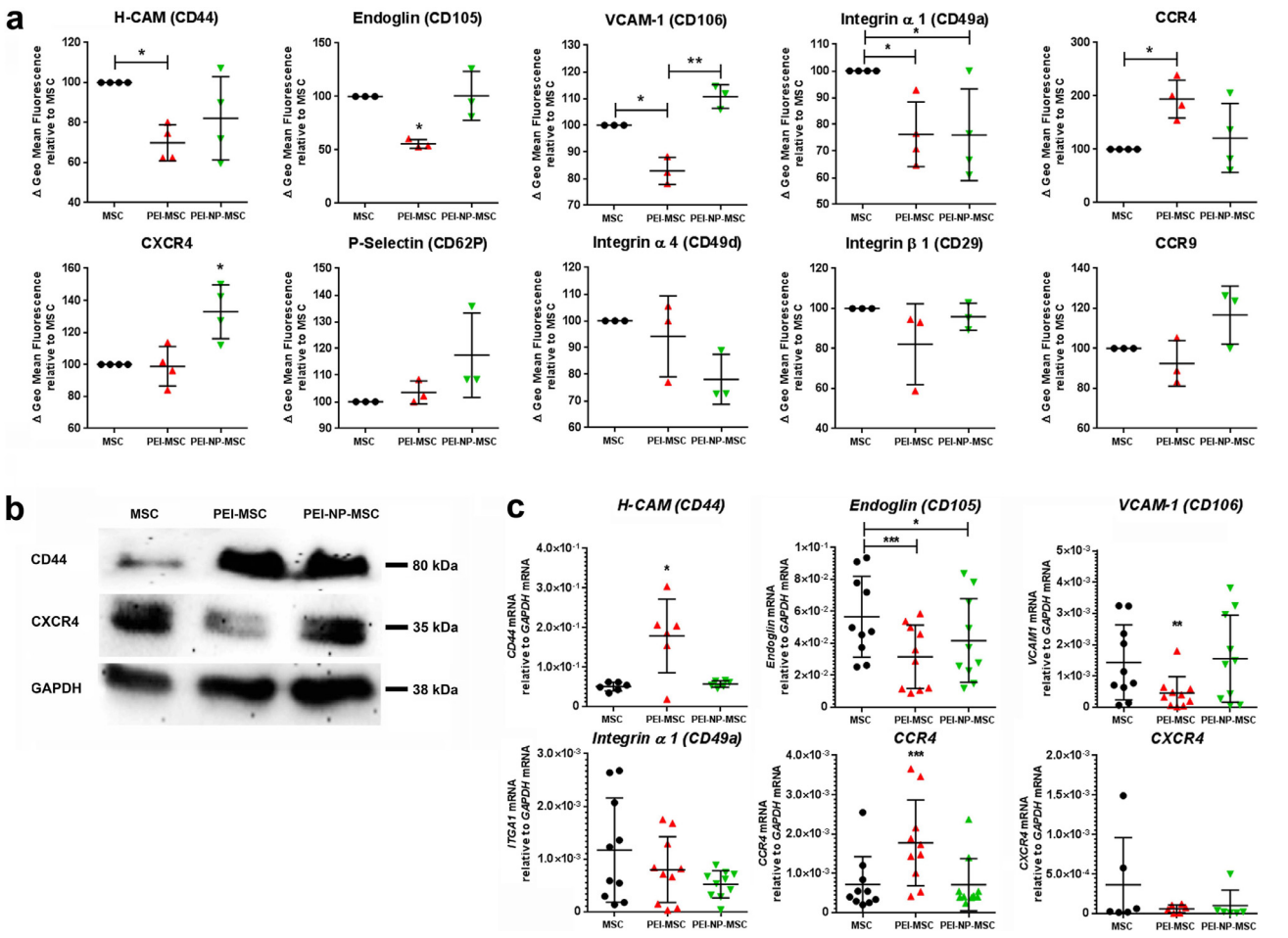

Fig. 1. Human MSC adhesion receptor and chemokine receptor analyses after PEI treatment and functional adhesion capacity assessment in vitro

(a) Expression levels of H-CAM (CD44), Endoglin (CD105), VCAM-1, VLA-1, VLA-4 (CD49d, β-1 integrin), P-selectin, CCR4, CCR9, and CXCR4 detected by flow cytometry in untreated human BM-MSC, and MSC treated with PEI alone or PEI-NP. $N = 3–4$, each data point represents one biological replicate per group; Flow cytometry data of untreated and PEI/NP treated MSC were compared with ANOVA followed by Tukey's multiple comparisons test ($^*p < 0.05$; $^{**}p < 0.01$). Error bars: SD.

(b) Western blot for CD44 and CXCR4 total protein in untreated MSC or treated with PEI alone or in combination with NP. Representative photograph of $N = 6$ biological replicates.

(c) Levels of indicated mRNAs measured by qPCR in untreated MSC or treated with PEI or PEI- NP ($N = 6–10$, each data point represents one biological replicate per group; replicates collectively analysed for the respective targets). mRNA expression data of untreated and PEI/NP treated MSC were compared with ANOVA followed by Tukey's multiple comparisons test ($^*p < 0.05$; $^{**}p < 0.01$; $^{***}p < 0.001$). Error bars: SD.

achieving maximal velocity after 260 s. Testing time was 300 s, and the time when the animal fell off the treadmill was used for statistical analysis. Further testing was done using the tight rope, for which mice were placed with their forepaws at the middle of a 60 cm long rope that was attached to two opposing platforms. Using a validated score between 0 (min) and 20 (max) the two parameters "platform arrival" and "time needed to reach the platform" were assessed. The test was performed twice per time point and means were calculated. For the corner turn test, two vertical boards forming an angle of 30° were used. Mice were placed into the test apparatus and the side chosen to leave the corner after contact with their vibrissae was analysed. Ten trials per test day were performed. Healthy unaffected mice randomly leave the corner, whereas mice suffering from cerebral ischemia leave the corner from the non-impaired (e.g., left) body side. The laterality index was calculated as (number of left turns – number of right turns) / 10.

2.27. Statistical analyses

All data are given as means ± standard deviation (SD) or standard error of means (SEM). Shapiro–Wilk test was applied to test normal distribution. For multiple comparisons of data obtained in vitro and in vivo (Fig. 1a,c; Fig. 2c,d; Fig. 3c; Fig. 4a,d; Suppl.Fig. 2a,b,e,f,g), one-way analysis of variance (ANOVA) followed by Tukey's post-hoc test was used. For single comparison in the other data sets the two-tailed t-test was employed. *P* values of <0.05 were considered to be statistically significant and are such listed in the Figure legends. For comparisons with low sample sizes (N≤4) descriptive statistics are listed in Supplementary Table 2.

3. Results

Functional blocking cell adhesion receptors and increasing CXCR4 expression modifies MSC adhesion to endothelial cells in vitro

First, we assessed homing and chemokine receptor expression on MSC in vitro. Untreated MSC did not express CCR1, CCR5, CCR6, CCR7, CXCR5, and CXCR6 (data not shown), and therefore, these receptors were not further analysed. PEI treatment of MSC impaired expression of CD44 (H-CAM), endoglin, CD106 (VCAM-1), and VLA-1 (integrin α1), but increased CCR4 expression dose-dependently. VLA-1 expression was also impaired upon PEI-NP treatment of MSC, but in contrast to PEI treatment, expression of VCAM-1 and CXCR4 were increased. Treatment of MSC with either PEI or PEI-NP did not affect the expression of P-selectin, VLA-4 (CD29, integrin β1), or CCR9 (Fig. 1a).

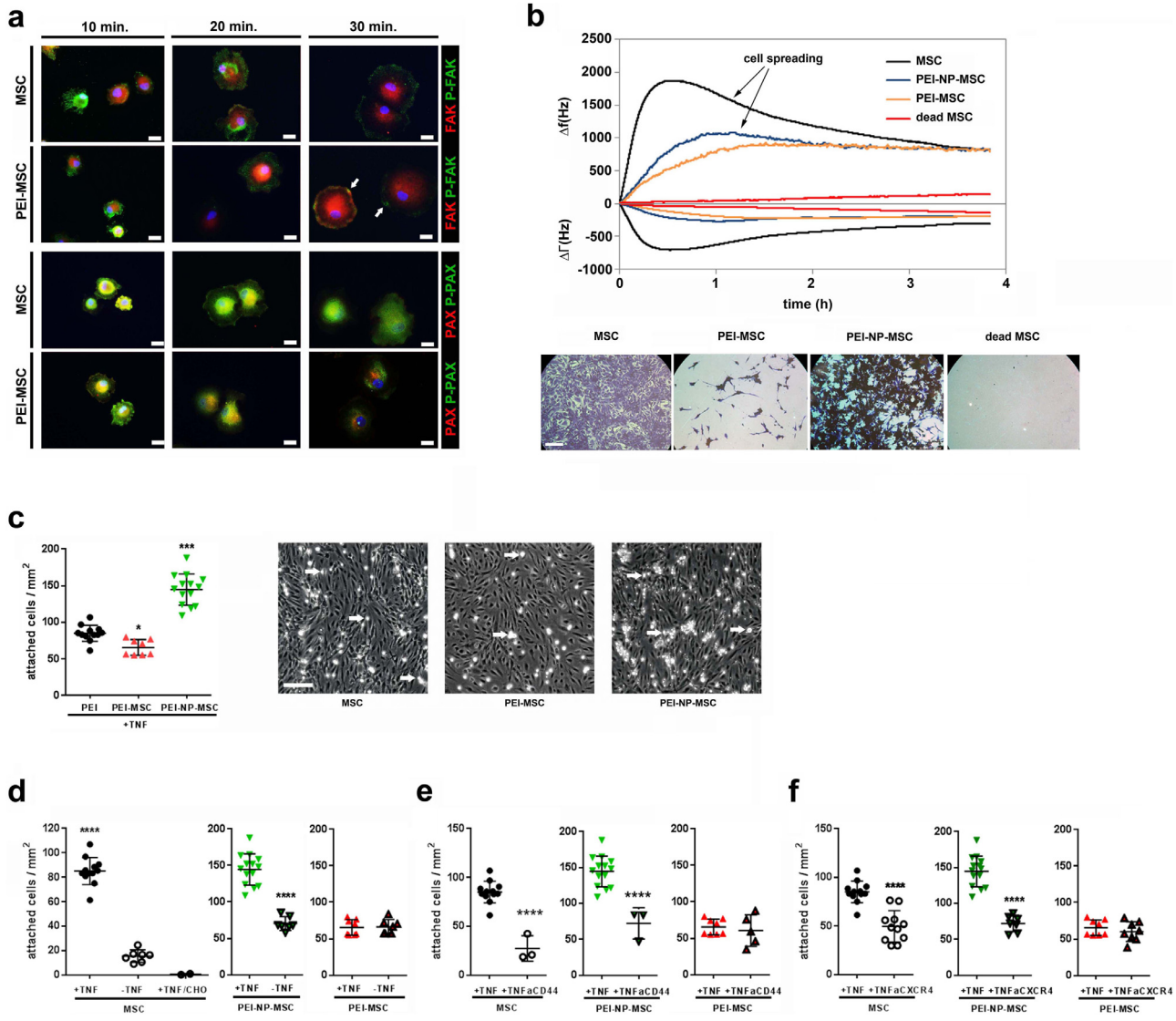

Fig. 2. Functional in vitro adhesion capacity of human MSC after PEI treatment

(a) In vitro integrin signalling analysis by immunocytochemistry of phosphorylated (green) and non-phosphorylated (red) focal adhesion point markers, focal adhesion kinase (FAK) and paxillin (PAX). PEI-MSC showed accelerated integrin signalling and focal adhesion points clustering differed over time between treated and untreated MSC. The focal adhesion points (arrows) of PEI-MSC appeared more evenly distributed and less accentuated. Scale bars: 20 μm. Microphotographs represent two technical replicates of pooled hBM-MSC (3 donors) per group out of a single experiment.

(b) Quartz Crystal Microbalance with Dissipation (QCM-D) experiments to evaluate seeding and spreading capacities of MSC upon PEI/NP treatment in real time. QCM-D measures surface adsorption by means of shifts in the resonance frequency (Δf) and damping behaviour (bandwidth, $\Delta\Gamma$) of an AT-cut quartz crystal. While a negative frequency shift is related to the amount of adsorbed mass, damping is the result of dissipative energy losses induced by the adsorbed mass. The relation between frequency and bandwidth represents the mass-sensor coupling, and a loosely coupled mass dissipates more energy (larger $\Delta\Gamma$) than a firmly coupled mass (smaller $\Delta\Gamma$). The figure displays representative graphs of three separate measurements for each condition. QCM-D data correlate with the microscopic images (crystal violet staining) taken after the mass sensitive measurements. Seeding density: 40,000 cells per sensor. Viable MSC can be distinguished from dead cells (negative control; 10 min. 57 °C; red graphs, right microphotograph in lower row) showing absence of significant frequency and bandwidth shifts; scale bar: 200 μm. Untreated viable MSC (black graphs) adhered within 30 minu with subsequent typical spreading signal (gradual decrease in bandwidth) in the following 4 hours. In contrast, PEI-MSC (yellow graphs) displayed slower adhesion and almost no spreading (stable bandwidth), indicating weaker adhesion. PEI-NP-MSC (blue graphs) also displayed slow adhesion, but typical spreading, although delayed and less pronounced than in MSC.

(c) Adhesion capacity of MSC and PEI/NP treated MSC under dynamic shear stress conditions to endothelial cells that were activated by TNFα. Flow chamber adhesion data of untreated and PEI/NP treated MSC were compared with ANOVA followed by Tukey's multiple comparisons test ($^{*}p < 0.05$; $^{***}p < 0.0001$). Error bars: SD. Arrows indicate exemplary adherent MSC; scale bar: 200 μm. N = 8–14, each data point represents the mean of cell counts of 5–12 individual experiments per group.

(d) Adhesion capacity of MSC and PEI/NP treated MSC under dynamic shear stress conditions to endothelial cells with or without TNFα activation as well as to CHO cells lacking intact adhesion molecules. Flow chamber adhesion data of untreated MSC with or without TNFα activation and to CHO cells were compared with ANOVA followed by Tukey's multiple comparisons test ($^{****}p < 0.001$); Flow chamber adhesion data of PEI/NP treated MSC with or without TNFα activation were compared with two-tailed t-test ($^{****}p < 0.0001$). Error bars: SD. N = 2 –12, each data point represents the mean of cell counts of 1 –8 individual experiments per group.

(e), (f) Adhesion capacity of MSC and PEI/NP treated MSC under dynamic shear stress conditions to endothelial cells with TNFα activation and blocking antibodies against CD44 or CXCR4. Flow chamber adhesion data of untreated and PEI/NP treated MSC with or without blocking antibodies were compared with two-tailed t-test ($^{****}p < 0.0001$). Error bars: SD. N = 3-14, each data point represents the mean of cell counts of 2 –9 individual experiments per group. (For interpretation of the references to colour in this figure legend, the reader is referred to the web version of this article.)

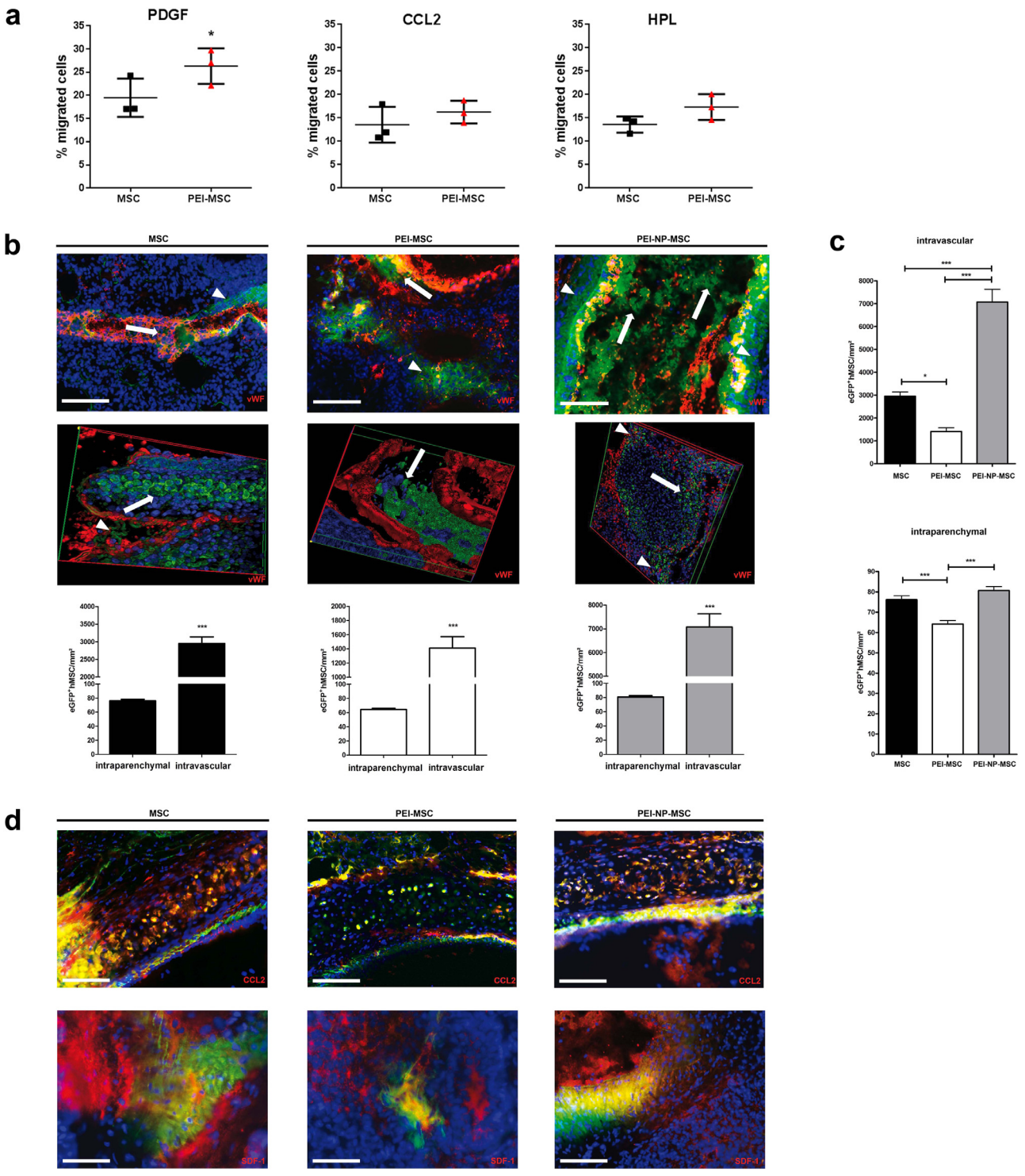

Fig. 3. Human MSC migration in vitro and their adhesion and migration in the lung in vivo

(a) Migration capacity expressed by % of untreated MSC and PEI treated MSC with or without additional chemoattractants or human platelet lysate (HPL). Migration data of untreated and PEI treated MSC were compared for each condition with two-tailed *t*-test (*$p < 0.05$), $N = 3$, each data point represents one biological replicate per group Error bars: SD.

(b) Immunofluorescence and associated quantification of MSC accumulation in the lung after intravenous application of 5×10^6 treated or untreated eGFP+ MSC in a rat model of unilateral hippocampal quinolinic acid (QA)-induced brain injury. Animals were sacrificed 24 h after application. Untreated and treated MSC were detected in the lumina of the small vessels (arrows), but also in close vicinity to the vessels (arrowheads). von Willebrand factor (vWF): red; GFP: green; DAPI: blue; scale bars: 100 μm. Intraparenchymal and intravascular cell numbers were compared for untreated MSC, PEI treated MSC or PEI-NP treated MSC with two-tailed unpaired *t*-test (***$p < 0.001$). $N = 3$ per group. Intravascular data represent 9 data points generated from 3 sections per mouse ($n = 3$). Intraparenchymal data represent 80 −180 data points generated from 6 to 9 micrographs from 8 to 30 sections. Error bars: SEM.

(c) Numbers of untreated MSC, PEI-MSC or PEI-NP-MSC detected in the vasculature and parenchyma. Cell numbers of untreated or PEI/NP treated MSC were compared for intraparenchymal or intravascular localisation with ANOVA followed by Tukey's multiple comparisons test (*$p < 0.05$, ***$p < 0.001$). $N = 3$ per group. Intravascular data represent 9 data points generated from 3 slides from $N = 3$ mice; intraparenchymal data represent 180 data points obtained from 30 slides per mouse (6 micrographs per section). Error bars: SEM.

(d) Immunofluorescence of CCL2 and SDF-1 in the pulmonary vasculature and parenchyma of rats administered with untreated MSC, PEI-MSC or PEI-NP-MSC. CCL2: red; GFP: green; DAPI: blue; scale bars: 100 μm SDF-1: red; GFP: green; DAPI: blue; scale bars: 50 μm (MSC, PEI-MSC), 100 μm (PEI-NP-MSC). (For interpretation of the references to colour in this figure legend, the reader is referred to the web version of this article.)

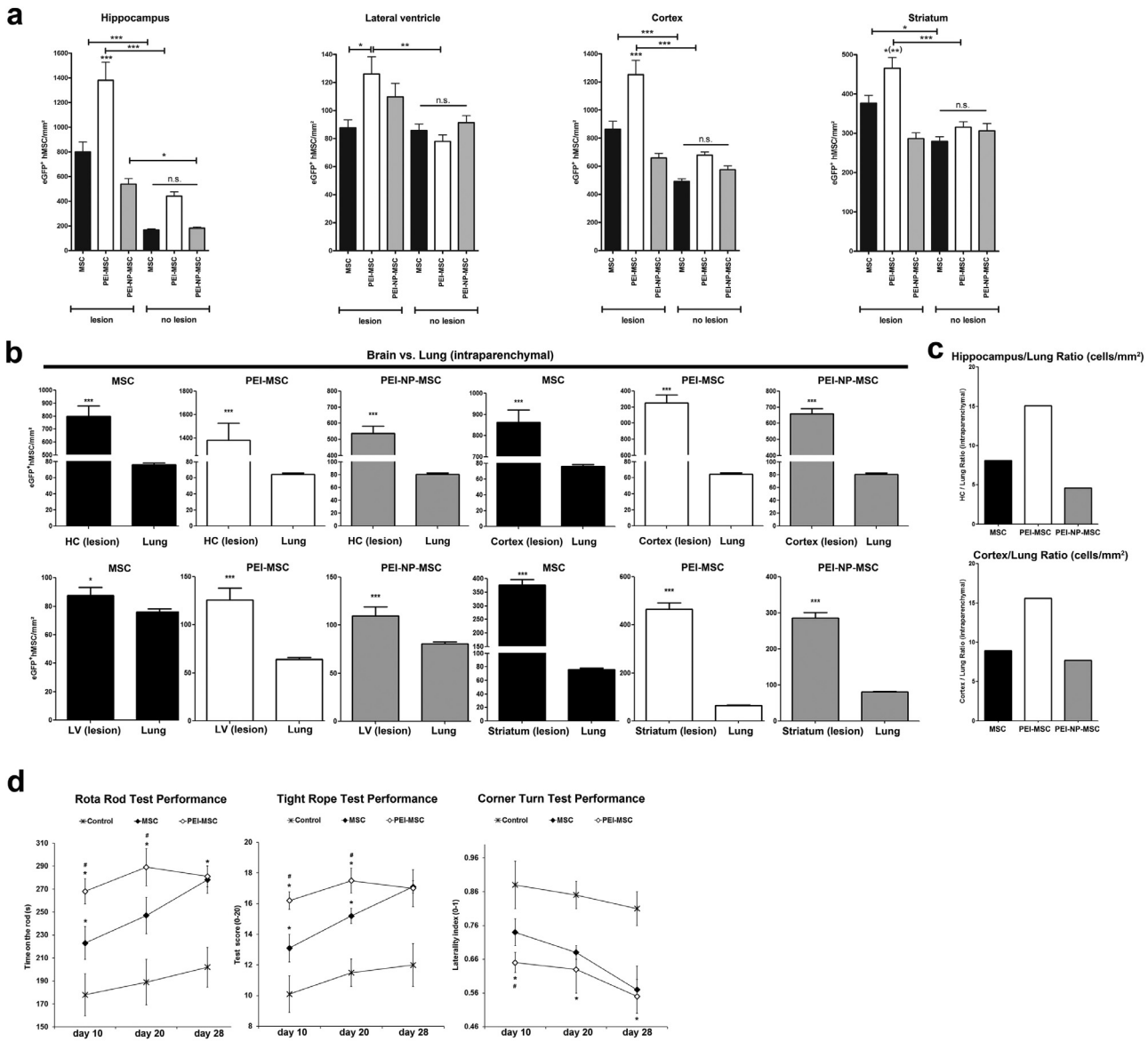

Fig. 4. Targeted homing of human MSC in the brain and their therapeutic efficacy

(a) Targeted homing of untreated MSC, PEI-MSC or PEI-NP-MSC assessed in different regions of the brain after intravenous application of 5×10^6 treated or untreated eGFP+ MSC to a rat model of unilateral hippocampal QA-induced brain injury. Treated or untreated MSC were applied 7 days after QA injury, and animals were sacrificed 24 h after application. Cell numbers of untreated or PEI/NP treated MSC were compared between lesioned and non-lesioned tissue as well as within lesioned and non-lesioned tissue in the different brain regions with ANOVA followed by Tukey's multiple comparisons test ($^*p < 0.05$, $^{**}p < 0.01$, $^{***}p < 0.001$). $N = 3$ per group. The columns represent 80–160 data points generated from 8 to 9 micrographs from 8 to 21 sections. Error bars: SEM.

(b) Quantification of untreated MSC, PEI-MSC or PEI-NP-MSC assessed in the parenchyma of the lesioned brain hemisphere (unilateral hippocampal QA-induced excitotoxic brain injury model), and the parenchyma of the non-lesioned lung. Intraparenchymal cell numbers in the lung and the different lesioned brain regions were compared for untreated or PEI/NP treated MSC with two-tailed *t*-test ($^*p < 0.05$; $^{***}p < 0.001$). $N = 3$ per group. The columns represent 80–180 data points generated from 6 to 9 micrographs from 8 to 30 sections. Error bars: SEM.

(c) Brain/lung ratio of untreated MSC, PEI-MSC or PEI-NP-MSC for hippocampus and cortex in the unilateral hippocampal QA-induced excitotoxic brain injury model.

(d) Analysis of motor coordination using the rotarod, the tight rope and the corner turn test in mice exposed to 45 min. of transient focal cerebral ischemia followed by intravenous transplantation of either eGFP+ MSC or eGFP+ PEI-MSC during reperfusion. A total of 1×10^6 cells were grafted per experimental condition. Controls received PBS only, $N = 7$ animals per group. Impairment of motor coordination was assessed on days 10, 20 and 28. Functional performance data of the groups received either PBS, untreated MSC, or PEI-MSC were compared with ANOVA followed by Tukey's multiple comparisons test (*significantly different from controls, $p < 0.05$; #significantly different from mice treated with MSC, $p < 0.05$) .

We observed an even distribution of CXCR4 molecules on the surface of untreated MSC and PEI-MSC (Supplementary Fig. 1). In contrast, the CXCR4 signal was strongly increased on the surface of PEI-NP-MSC where it appeared in condensed patterns that co-localized with the PEI-NP complexes, indicating a mechanistic impact of NP deposits on CXCR4 protein expression (Fig. 1a; Supplementary Fig. 1). PEI treatment alone resulted in decreased expression of total CXCR4 protein (intracellular and on the MSC surface), but combined treatment of MSC did not affect either *CXCR4* mRNA or CXCR4 total protein expression, suggesting a post-translational regulation of CXCR4 on the surface of PEI-NP-MSC (Fig. 1b,c; Supplementary Fig. 1b). MSC treatment with either PEI or PEI-NP resulted in increased expression of CD44 total protein, whereas only PEI treatment increased *CD44* mRNA levels (Fig. 1b,c). Soluble CD44 protein was not detected in the supernatants of untreated or treated MSC, only insoluble CD44 in the MSC lysate. This indicates that the decreased

detectability of CD44 molecules on the surface of PEI-MSC was mediated by cationic interaction of PEI with membrane bound CD44 molecules rather than by splitting off the soluble CD44 fraction (Supplementary Table 1). Significant changes of *CCR4, endoglin*, and *VCAM-1* mRNA were also observed, confirming a transcriptional effect of PEI treatment (Fig. 1c). PEI/NP treatment impacted the production and secretion of trophic factors and EV release, but not the expression of CD10, CD140b, GD2, or PDPN proteins on MSC, or MSC viability, tri-lineage differentiation potential, or immunomodulatory capacity (Supplementary Fig. 2,3).

Next, we investigated the functional impact of PEI/NP treatment on MSC adhesion. Integrin signalling was accelerated in PEI-MSC, which had weaker focal adhesion points (Fig. 2a). PEI treatment caused adherent MSC to cover a smaller surface area than untreated MSC, suggesting that PEI has a membrane condensation effect. In contrast, PEI treatment did not affect the size of detached MSC (Supplementary Fig. 2b, 4). In addition, PEI-MSC featured delayed adhesion kinetics, and quartz crystal microbalance with dissipation analysis revealed impaired seeding and spreading capacities of MSC upon PEI treatment (Fig. 2b; Supplementary Fig. 4).

Under dynamic shear stress, modelling the physical stress to which MSC are exposed after intravascular administration, PEI treatment of MSC decreased their adhesion capacity to endothelial cells (EC), whereas PEI-NP-MSC showed increased adhesion. This suggested that PEI treatment not only reduced the detectability of MSC adhesion receptors but also blocked their functions, and that the higher expressed CXCR4 molecules on PEI-NP-MSC were functional as well. Depletion of TNFα and antibody-mediated blocking of CD44 and CXCR4 reduced the adhesion of MSC and PEI-NP-MSC to EC, but did not further reduce the already impaired adhesion capacity of PEI-MSC (Fig. 2c–f). This confirmed the functional relevance of adhesion molecules and the interactions with their ligands on EC for the modulation of stem cell adhesion.

3.1. PEI treatment modifies MSC migration in vitro

Exiting the vasculature into the surrounding tissue is a crucial step in stem cell homing. Therefore, we analysed the MSC transmigration ability in vitro. PEI treatment increased MSC migration in the presence of PDGF, CCL2 or human platelet lysate (HPL) indicating the involvement of multiple mechanisms beyond the CCL2-CCR4 axis in PEI-MSC migration (Fig. 3a). To address MSC functional heterogeneity, we explored the susceptibility of distinct MSC subpopulations to PEI treatment with respect to their migration capacities. PEI treatment promoted migration of CCR4+ and CD140b+ subpopulations but either did not promote or even reduced migration of CD10+ and GD2+ subpopulations (Supplementary Fig. 5).

Functional blocking of cell adhesion receptors modulates MSC adhesion to lung endothelium after systemic administration

We hypothesized that adhesion to the lung endothelium could limit the effect of stem cell therapies, and, therefore investigated whether PEI treatment could circumvent that. Hence, we intravenously administered eGFP+ MSC, PEI-MSC and PEI-NP-MSC to a rat model of unilateral hippocampal quinolinic acid (QA)-induced excitotoxic injury. We found untreated MSC, PEI-MSC and PEI-NP-MSC in the lumina of the small pulmonary vessels and in close vicinity to the vessels, indicating transmigration towards the lung parenchyma (Fig. 3b). In line with their reduced adhesion rate to EC in vitro, significantly fewer PEI-MSC were detected in the vessels and in the lung parenchyma. In contrast, the number of PEI-NP-MSC in the vessels was higher compared to untreated MSC or PEI-MSC (Fig. 3c). To investigate the involvement of the molecules that were induced by PEI/NP treatment in vitro we next analysed the ligands of CCR4, i.e. CCL2, and CXCR4, i.e. SDF-1, in the lung as well as their possible interactions with the transplanted MSC. Immunostaining of the pulmonary vessel walls demonstrated that PEI-MSC showed less interaction with CCL2 in the lung, likely due to their impaired adhesion capacity (Fig. 3d). Our results indicate that PEI treatment of MSC reduces their adhesion to endothelial cells and thereby their accumulation in blood vessels in vivo, which could enhance their therapeutic efficacy.

Functional blocking of cell adhesion receptors and increasing CCR4 expression results in MSC targeted homing and improves their therapeutic efficacy after systemic administration

We next tested directly whether the decreased EC adhesion indeed translated to improved delivery to the target area using the unilateral QA brain injury rat model. This model was chosen because of the known feature of QA to increase SDF-1 and CCL2 in astroglia [38]. We found higher concentrations of the CCR4 ligand CCL2, and the attractants MIP-1a and IP-10, indicating the presence of an inflammatory milieu to attract systemically administered eGFP+ MSC to the brain (Supplementary Figs. 6 and 7). We detected more transplanted MSC in the lesioned hemisphere confirming the known MSC tropism towards tissue injury [4]. Due to their reduced first pass accumulation in the lung we expected to find more PEI-MSC than untreated MSC in the brain lesion. Indeed, within the lesioned brain tissue, the number of PEI-MSC was strongly increased compared to the number of untreated MSC and PEI-NP-MSC. No differences of the homing patterns of treated or untreated MSC were observed in non-lesioned brain areas (Fig. 4a). After i.v. application, PEI-MSC had improved migration potential in the brain compared to the lung (Fig. 4b,c).

We also analysed the effect of PEI treatment of MSC on recovery using a ischemic stroke mouse model, whereby mice are exposed to 45 min. of transient focal cerebral ischemia followed by intravenous transplantation of either eGFP+ MSC or eGFP+ PEI-MSC during reperfusion. Although both i.v. administered MSC and PEI-MSC improved recovery of mice after stroke, PEI-MSC performed significantly better than untreated MSC at acute and subacute disease stages (Fig. 4d). Further, neuronal, glial and oligodendrocyte markers were detected in close vicinity to PEI-MSC and untreated MSC, with a trend to higher co-expression in PEI-MSC (Supplementary Fig. 8), indicating that the targeted PEI-MSC were stimulating tissue repair.

In the QA injury model, MSC were found in close proximity to the brain vasculature where, contrary to the lung, most MSC transmigrated from the vessel lumen towards the parenchyma (Supplementary Fig. 7a). In the lesioned brain in particular, PEI-MSC accumulated in areas of high CCL2 protein expression, which is a pro-migratory protein (Supplementary Fig. 7b). To understand the mechanism underlying the increased MSC migration potential in the lesioned brain compared to the lung, we analysed the levels of CCL2 and other pro-migratory proteins. Unexpectedly, we detected much higher concentrations of pro-migratory proteins in the lungs than in the brains of QA injury and haemorrhagic stroke (SP-SHR) models as well as in healthy rats (Supplementary Fig. 9). We also asked if the lung and brain EC, as “gatekeepers” of MSC transmigration from the vasculature into the tissue, might feature different contents of pro-migratory factors. Indeed, more CCL2 and TGFβ were detected in brain EC than in lung EC (Supplementary Fig. 10). Thus, we conclude that lung EC, expressing lower amounts of pro-migratory factors and effectively separating the transplanted cells from the cytokines located beneath the intact EC layer, play a relevant role in the decreased MSC transmigration rate in the lung compared to the lesioned brain.

Altogether, we propose that suppression of PEI-MSC adhesion to lung EC decreases accumulation of PEI-MSC in the lung and, together with increased CCR4 expression, enables increased targeted homing to the lesioned brain tissue.

3.2. PEI treatment modifies MSC migration in vivo

As MSC show tumour tropism [4], we finally assessed the MSC`s trans-hemispheric migration rate towards previously implanted glioblastoma cells to validate their in vivo migration capacities. More

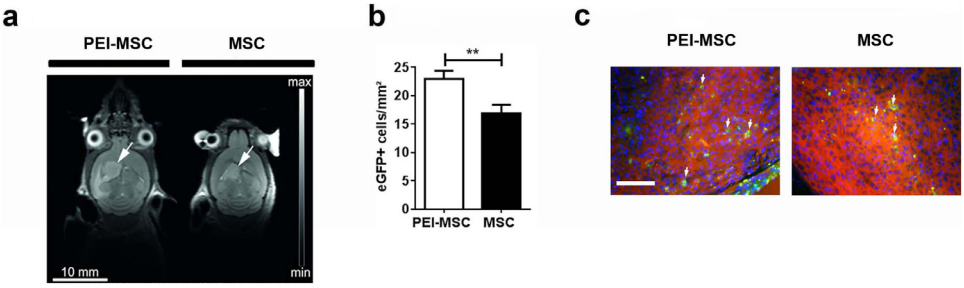

Fig. 5. In vivo intracerebral application of migration- and adhesion-modulated MSC in an orthotopic model of glioblastoma

(a) 1×10^5 ds-red-U87MG cells were injected into the brain of NMRI mice, and a T2-weighted MR-anatomy acquired 18 days post injection of ds-red-U87MG cells. 1×10^5 eGFP + MSC or eGFP+ PEI-MSC were injected into the contralateral side on day 22 after intracerebral injection of the ds-red-U87MG cells. Tumours are indicated with arrows.

(b) Quantification of eGFP+ MSC and eGFP+ PEI-MSC in the tumor area 6 days after intracerebral injection of GFP-MSC ($N = 4$ per group). The columns represent 63 or 111 data points obtained from 20 to 25 sections per mouse brain (3–4 micrographs analysed per section). Cell numbers of untreated MSC and PEI-MSC were compared with two-tailed *t*-test (**$p < 0.01$); Error bars: SEM.

(c) eGFP+ MSC and eGFP+ PEI-MSC (green) highlighted with arrows in the ds-red-U87MG (red cells) tumour area 28 days after intracerebral injection of ds-red-U87MG and 6 days after injection of 1×10^5 eGFP+ MSC or eGFP+PEI-MSC into the contralateral hemisphere. Scale bar: 100 μm. (For interpretation of the references to colour in this figure legend, the reader is referred to the web version of this article.)

PEI-MSC migrated to the tumours than untreated MSC confirming the observed increase of the in vitro MSC migration capacity by PEI treatment. This provides further evidence for their superior in vivo migration capacities and confirms migration through tissue as a relevant mechanism for stem cell therapies´efficacy (Fig. 5).

4. Discussion

The present study shed light on the factors influencing MSC homing to the brain from the mechanistic perspective of adhesion- and transendothelial migration as key tools that can be modulated for increased and sustained delivery efficacy of systemically administered stem cells. Furthermore, our data strongly suggest that modulating cell surface properties, as exemplified by PEI treatment, can help not only to escape the stem cell entrapment in the lung vessels, but also to promote their migration within the targeted organ evidenced by improved homing and therapeutic efficacy in in vivo models of brain injury.

Particularly MSC are being evaluated as a promising cell therapy source for various clinical applications due to their powerful immunomodulatory and regenerative potential [39].

Despite featuring chemokine-mediated tropism toward lesioned or inflamed tissue, previous studies reported that only few of systemically applied MSC home to the target tissue with the majority of the cells being “trapped” in parenchymal organs such as the lung [4,40].

The observation that a stem cell transplant can exert some therapeutic effects even when most of the cells do not reach the damaged organ has led to the hypothesis that these cells systemically release regenerative or immunomodulatory factors that may sufficiently repair the local damage such as an infarcted heart or brain [11].

However, the sustainable implementation of stem cell therapies is still hampered by their inconsistent efficacies, and it is reasonable to assume that the loss of many of the transplanted cells to non-lesioned organs or tissue is a relevant cause for this shortcoming. Moreover, such first-passage filtering of stem cells from the circulation to non-lesioned tissue can be dangerous for various organs, e.g. leading to cerebral or pulmonary embolism [9,41]. Thus, directing the transplanted cells to the target region could reduce side effects and improve the therapeutic efficacy of the stem cell graft. We show that targeting stem cell homing by modulating cell adhesion and chemokine receptors can enhance their therapeutic efficacy.

PEI-MSC showed lower detectability/expression of the integrin subunit CD49a, endoglin, CD44 and VCAM-1, and decreased adhesion to EC under dynamic shear stress conditions. Further, our observations using blocking antibodies indicate that CD44 and CXCR4 are not substantially involved in PEI-MSC interactions with EC, and that PEI decreases the adhesion of MSC on EC regardless of EC’s activation status. A compensatory increase in *CD44* mRNA and CD44 protein on PEI treatment indicates a potential feedback to CD44 molecules impairment on the MSC surface. Moreover, PEI appears to disrupt the interaction of CD44 molecules with their natural ligands on the EC surface and with anti-CD44 antibodies, without inducing CD44 cleavage on MSC [42]. Cationic agents can interfere with signalling pathways such as suppression of TNFα-induced VCAM-1 expression [43]. Moreover, CD44 is involved in the expression of chemokines and receptors such as CXCR5 [44]. The increased CCR4 expression in PEI-MSC can be explained by intracellular PEI effects, including interactions with negatively charged DNA and/or RNA, possibly also involving CD44, with the regulatory pathways of CCR4 that remain to be further elucidated.

Pro-inflammatory cytokines are potent attractors for MSC [5,20], and they can migrate toward the lesioned striatum in the 6-hydroxydopamin PD model [45]. Similarly, in the QA lesion model we detected higher concentrations of pro-inflammatory chemokines in the lesioned hemisphere. As CCR4 expression was increased on PEI-MSC we hypothesized that its ligand CCL2 plays a substantial role in their increased homing capacity. We confirmed the increased expression of CCL2 in the lesion, hereby identifying the CCR4-CCL2 axis, additionally to the previously described CCR2-CCL2 axis [46], as a contributor to stem cell homing. Previously, it was reported that integrins are involved in the entrapment of MSC in the lung [6]. Our data confirm that MSC accumulation in the lung is not merely the result of MSC congesting small pulmonary vessels but also depends on the function of their adhesion receptors.

We conclude that the targeted homing of PEI-MSC to the site of injury after systemic application was enhanced by their lower adhesion capacity to inactivated EC without compromised chemokine receptors but increased CCR4 expression. The observed condensation effects of PEI treatment on the MSC membrane may have further facilitated their passage through the small vessels of the lung.

We excluded non-specific MSC adhesion to EC by iron NP complexes as treated or untreated MSC did not attach to CHO-A5 cells, yet mechanical force can increase CXCR4 expression on stem cell surfaces [13]. Thus, NP complexes, acting as mechanical stimuli, are likely to trigger “in-side-out flipping” of CXCR4 molecules thereby increasing MSC adhesion capacity. The increased adhesion potential of PEI-NP-MSC might be suitable for local stem cell applications preventing the undesired migration of the stem cell graft through the vasculature toward non-lesioned regions.

PEI-MSC featured increased secretion and/or production of trophic factors suggesting the possible optimization of MSC therapeutic effects. Indeed, we observed a significant improvement early after

stroke in the PEI-MSC group compared to untreated MSC. At the end of the observation period the in vivo effects of both groups converged, performing equally better than vehicle controls. At this time the numbers of PEI-MSC and untreated MSC were not significantly different in the post mortem analyses, likely due to secondary stem cell loss in the ischemic extracellular milieu [33], highlighting the relevance of (stem) cells` homing for their therapeutic efficacy.

Blocking CXCR4 or CD44 on PEI-NP-MSC did not reduce their adhesion rates below controls, and it is likely that the PEI+/-NP effects are not restricted to the receptors and factors we analysed but might also apply to a greater variety of molecules located on the cell surface and in the cytoplasm of transplanted MSC, as well as in the host vasculature and tissue. In order to identify possible effects of PEI on other extracellular and cytoplasmic molecules, a broad proteomic screening including integrins, PECAM-1, ICAM-1, E-/L-selectin, and glycoproteins should be considered for future studies. Also, other cationic agents such as cationic click polymers, lipids, polysaccharides, or salts may be worthy candidates for thorough evaluation of their impact on stem cell homing.

We modulated the adhesion and migration capacities of MSC and found that this increased their targeted homing rates by reducing the first-passage filtering in the lung, and, notably, improved their therapeutic efficacy. Moreover, beyond its adhesion-modulating role, PEI treatment enhanced the tumour tropism of intracerebrally injected MSC hereby confirming its impact on stem cell in vivo migration potential. This finding is of particular interest for implementation of MSC as delivery vehicles for oncolytic adenoviral therapy, particularly acknowledging the high variability of MSC's tumour tropism across different glioma models and delivery routes [4].

We validated our findings in vitro as well as in vivo in preclinical small animal models including stroke. Yet, rodent models assessing vascular cognitive impairment may be limited due to differences to larger animals or human, such as paucity of white matter [47], suggesting further validation in larger species is necessary. Moreover, a clinical monitoring of the stem cell grafts distribution, e.g. applying non-invasive imaging technologies, would be valuable to track the fate of the graft in the patient. This may not only allow to assess an individual efficacy profile, but also help to reduce, or even prevent, side effects. Specifically, iron or gadolinium-(NP) labelled stem cells can be detected by MRI [48,49], or, more recently, advanced approaches were developed using reporter gene imaging that could combine graft tracking with its functional assessment such as viability or therapeutic capacities [50].

The concept described here elucidates the interactions of stem cell transplants with lesioned and non-lesioned host tissue, specifically pulmonary endothelium and brain tissue. Hereby, we identified the adhesion of transplanted stem cells to endothelium and their migration capacity as relevant MoAs for their therapeutic efficacy. This paves the way towards future production of customized cellular grafts for respective clinical indications in regenerative medicine and oncology, thereby contributing to realizing the full potential of (stem) cell therapies.

4.1. Data sharing

Materials used in this study are commercially available. Study-specific primary cell material can be provided upon availability and written request to the corresponding authors and signed material transfer agreement.

Funding sources

This work was supported in part by the Robert Bosch Stiftung (Stuttgart, Germany) given to M.S., by the IZEPHA grant given to L.D., as well as by a Commission of the European Communities Grant 7th FP Health (grant number: 223236 [CASCADE]) given to R.S. The funders had no role in study design, data collection, data analysis, or interpretation.

Authors` contributions

R.S. and L.D. designed the research, analysed the data and wrote the manuscript. A.K., A.v.A-M., A.L., M.B., D.G., M.A.K, C.C.A.E., A.K.F., F. K.G., R.K., G.G., J.S., K. Barth, K. Bieback, G. Siegel, G. Spohn, and E. Scheer performed the experiments, analysed the data and reviewed the manuscript. M.S., H-P.W., M.D., T.R.D., D.M.H., E-M.A., S.E., J. Schmehl, C.D.C., E.S., and H.N. discussed the results and reviewed the manuscript. T.K. provided human BM and reviewed the manuscript. All authors read and approved the final version of the manuscript

Declaration of Competing Interest

Dr. Danielyan reports grants from IZEPHA, during the conduct of the study. Dr. Schwab reports grants from Robert Bosch Stiftung (Stuttgart, Germany) during the conduct of the study. Dr. Schäfer reports a grant from the Commission of the European Communities during the conduct of the study. Dres Schäfer, Danielyan, von Ameln-Mayerhofer, Wendel, Kluba, Dominici, Claussen, Northoff and Siegel have a patent DE102012111891.4.; EP13801557.3. Dr. Gehring is a shareholder of 3T analytic. All other authors have no competing interests.

Acknowledgements

The authors wish to thank Ursula Hermanutz-Klein, Monika Hirlinger, Liane Spranger, Oksana Faul, Adam L.J. Olsson, Susanne Elvers-Hornung, and Christin Riegel for technical assistance, as well as Life Science Editors for editorial assistance.

Supplementary materials

Supplementary material associated with this article can be found in the online version at doi:10.1016/j.ebiom.2020.102987.

References

[1] Tewary M, Shakiba N, Zandstra PW. Stem cell bioengineering: building from stem cell biology. Nat Rev Genet 2018;19(10):595–614.
[2] D'souza N, Rossignoli F, Golinelli G, Grisendi G, Spano C, Candini O, et al. Mesenchymal stem/stromal cells as a delivery platform in cell and gene therapies. BMC Med 2015;13:186.
[3] Nitzsche F, Muller C, Lukomska B, Jolkkonen J, Deten A, Boltze J. Concise review: MSC adhesion cascade-insights into homing and transendothelial migration. Stem Cells 2017;35(6):1446–60.
[4] Krueger TEG, Thorek DLJ, Denmeade SR, Isaacs JT, Brennen WN. Concise review: mesenchymal stem cell-based drug delivery: the good, the bad, the ugly, and the promise. Stem Cells Transl Med 2018;7(9):651–63.
[5] Karp JM, Leng Teo GS. Mesenchymal stem cell homing: the devil is in the details. Cell Stem Cell 2009;4(3):206–16.
[6] Wang S, Guo L, Ge J, Yu L, Cai T, Tian R, et al. Excess integrins cause lung entrapment of mesenchymal stem cells. Stem Cells 2015;33(11):3315–26.
[7] Nystedt J, Anderson H, Tikkanen J, Pietila M, Hirvonen T, Takalo R, et al. Cell surface structures influence lung clearance rate of systemically infused mesenchymal stromal cells. Stem Cells 2013;31(2):317–26.
[8] Leibacher J, Henschler R. Biodistribution, migration and homing of systemically applied mesenchymal stem/stromal cells. Stem Cell Res Ther 2016;7:7.
[9] Cui LL, Kerkela E, Bakreen A, Nitzsche F, Andrzejewska A, Nowakowski A, et al. The cerebral embolism evoked by intra-arterial delivery of allogeneic bone marrow mesenchymal stem cells in rats is related to cell dose and infusion velocity. Stem Cell Res Ther 2015;6:11.
[10] Toma C, Wagner WR, Bowry S, Schwartz A, Villanueva F. Fate of culture-expanded mesenchymal stem cells in the microvasculature: in vivo observations of cell kinetics. Circ Res 2009;104(3):398–402.
[11] Lee RH, Pulin AA, Seo MJ, Kota DJ, Ylostalo J, Larson BL, et al. Intravenous hMSCs improve myocardial infarction in mice because cells embolized in lung are activated to secrete the anti-inflammatory protein TSG-6. Cell Stem Cell 2009;5(1):54–63.
[12] Leibacher J, Dauber K, Ehser S, Brixner V, Kollar K, Vogel A, et al. Human mesenchymal stromal cells undergo apoptosis and fragmentation after intravenous application in immune-competent mice. Cytotherapy 2017;19(1):61–74.

[13] Ruster B, Gottig S, Ludwig RJ, Bistrian R, Muller S, Seifried E, et al. Mesenchymal stem cells display coordinated rolling and adhesion behavior on endothelial cells. Blood 2006;108(12):3938–44.
[14] Docheva D, Popov C, Mutschler W, Schieker M. Human mesenchymal stem cells in contact with their environment: surface characteristics and the integrin system. J Cell Mol Med 2007;11(1):21–38.
[15] Potapova IA, Brink PR, Cohen IS, Doronin SV. Culturing of human mesenchymal stem cells as 3D-aggregates induces functional expression of CXCR4 that regulates adhesion to endothelial cells. J Biol Chem 2008.
[16] Honczarenko M, Le Y, Swierkowski M, Ghiran I, Glodek AM, Silberstein LE. Human bone marrow stromal cells express a distinct set of biologically functional chemokine receptors. Stem Cells 2006;24(4):1030–41.
[17] Cheng Z, Ou L, Zhou X, Li F, Jia X, Zhang Y, et al. Targeted migration of mesenchymal stem cells modified with CXCR4 gene to infarcted myocardium improves cardiac performance. Mol Ther 2008;16(3):571–9.
[18] Kumar S, Ponnazhagan S. Bone homing of mesenchymal stem cells by ectopic alpha 4 integrin expression. FASEB J 2007;21(14):3917–27.
[19] Sackstein R, Merzaban JS, Cain DW, Dagia NM, Spencer JA, Lin CP, et al. Ex vivo glycan engineering of CD44 programs human multipotent mesenchymal stromal cell trafficking to bone. Nat Med 2008;14(2):181–7.
[20] Sarkar D, Spencer JA, Phillips JA, Zhao W, Schafer S, Spelke DP, et al. Engineered cell homing. Blood 2011;118(25):e184–91.
[21] Kerkela E, Hakkarainen T, Makela T, Raki M, Kambur O, Kilpinen L, et al. Transient proteolytic modification of mesenchymal stromal cells increases lung clearance rate and targeting to injured tissue. Stem Cells Transl Med 2013;2(7):510–20.
[22] Zhu H, Mitsuhashi N, Klein A, Barsky LW, Weinberg K, Barr ML, et al. The role of the hyaluronan receptor CD44 in mesenchymal stem cell migration in the extracellular matrix. Stem Cells 2006;24(4):928–35.
[23] Tiwari S, Askari JA, Humphries MJ, Bulleid NJ. Divalent cations regulate the folding and activation status of integrins during their intracellular trafficking. J Cell Sci 2011;124(Pt 10):1672–80.
[24] Campbell ID, Humphries MJ. Integrin structure, activation, and interactions. Cold Spring Harb Perspect Biol 2011;3(3).
[25] Whiss PA, Andersson RG. Divalent cations and the protein surface co-ordinate the intensity of human platelet adhesion and P-selectin surface expression. Blood Coagul Fibrinolysis 2002;13(5):407–16.
[26] Schafer R, Kehlbach R, Muller M, Bantleon R, Kluba T, Ayturan M, et al. Labeling of human mesenchymal stromal cells with superparamagnetic iron oxide leads to a decrease in migration capacity and colony formation ability. Cytotherapy 2009:1–11.
[27] Siegel G, Kluba T, Hermanutz-Klein U, Bieback K, Northoff H, Schafer R. Phenotype, donor age and gender affect function of human bone marrow-derived mesenchymal stromal cells. BMC Med 2013;11:146.
[28] Marx JC, Allay JA, Persons DA, Nooner SA, Hargrove PW, Kelly PF, et al. High-efficiency transduction and long-term gene expression with a murine stem cell retroviral vector encoding the green fluorescent protein in human marrow stromal cells. Hum Gene Ther 1999;10(7):1163–73.
[29] Grisendi G, Bussolari R, Cafarelli L, Petak I, Rasini V, Veronesi E, et al. Adipose-derived mesenchymal stem cells as stable source of tumor necrosis factor-related apoptosis-inducing ligand delivery for cancer therapy. Cancer Res 2010;70(9):3718–29.
[30] Brown SA, Fleury-Olela F, Nagoshi E, Hauser C, Juge C, Meier CA, et al. The period length of fibroblast circadian gene expression varies widely among human individuals. PLoS Biol 2005;3(10):e338.
[31] Stegmeier F, Hu G, Rickles RJ, Hannon GJ, Elledge SJ. A lentiviral microRNA-based system for single-copy polymerase II-regulated RNA interference in mammalian cells. Proc Natl Acad Sci USA 2005;102(37):13212–7.
[32] Lindl T, Lewandowski B, Schreyogg S, Staudte A. An evaluation of the in vitro cytotoxicities of 50 chemicals by using an electrical current exclusion method versus the neutral red uptake and MTT assays. Altern Lab Anim 2005;33(6):591–601.
[33] Doeppner TR, Ewert TA, Tonges L, Herz J, Zechariah A, ElAli A, et al. Transduction of neural precursor cells with TAT-heat shock protein 70 chaperone: therapeutic potential against ischemic stroke after intrastriatal and systemic transplantation. Stem Cells 2012;30(6):1297–310.
[34] Walker T, Muller I, Raabe C, Nohe B, Zanke C, Ziemer G, et al. Effective silencing of adhesion molecules on venous endothelial cells for protection of venous bypass grafts. Eur J Cardiothorac Surg 2011;40(5):1241–7.
[35] Dreher L, Elvers-Hornung S, Brinkmann I, Huck V, Henschler R, Gloe T, et al. Cultivation in human serum reduces adipose tissue-derived mesenchymal stromal cell adhesion to laminin and endothelium and reduces capillary entrapment. Stem Cells Dev 2013;22(5):791–803.
[36] Doeppner TR, Kaltwasser B, Bahr M, Hermann DM. Effects of neural progenitor cells on post-stroke neurological impairment-a detailed and comprehensive analysis of behavioral tests. Front Cell Neurosci 2014;8:338.
[37] Doeppner TR, Kaltwasser B, Teli MK, Bretschneider E, Bahr M, Hermann DM. Effects of acute versus post-acute systemic delivery of neural progenitor cells on neurological recovery and brain remodeling after focal cerebral ischemia in mice. Cell Death Dis 2014;5:e1386.
[38] Guillemin GJ, Croitoru-Lamoury J, Dormont D, Armati PJ, Brew BJ. Quinolinic acid upregulates chemokine production and chemokine receptor expression in astrocytes. Glia 2003;41(4):371–81.
[39] Schafer R. Advanced cell therapeutics are changing the clinical landscape: will mesenchymal stromal cells be a part of it? BMC Med 2019;17(1):53.
[40] Phinney DG, Pittenger MF. Concise review: MSC-derived exosomes for cell-free therapy. Stem Cells 2017;35(4):851–8.
[41] Sugiyama Y, Sato Y, Kitase Y, Suzuki T, Kondo T, Mikrogeorgiou A, et al. Intravenous administration of bone marrow-derived mesenchymal stem cell, but not adipose tissue-derived stem cell, ameliorated the neonatal hypoxic-ischemic brain injury by changing cerebral inflammatory state in rat. Front Neurol 2018;9:757.
[42] Okamoto I, Tsuiki H, Kenyon LC, Godwin AK, Emlet DR, Holgado-Madruga M, et al. Proteolytic cleavage of the CD44 adhesion molecule in multiple human tumors. Am J Pathol 2002;160(2):441–7.
[43] Maus U, Rosseau S, Mandrakas N, Schlingensiepen R, Maus R, Muth H, et al. Cationic lipids employed for antisense oligodeoxynucleotide transport may inhibit vascular cell adhesion molecule-1 expression in human endothelial cells: a word of caution. Antisense Nucleic Acid Drug Dev 1999;9(1):71–80.
[44] Lisignoli G, Cristino S, Piacentini A, Cavallo C, Caplan AI, Facchini A. Hyaluronan-based polymer scaffold modulates the expression of inflammatory and degradative factors in mesenchymal stem cells: Involvement of Cd44 and Cd54. J Cell Physiol 2006;207(2):364–73.
[45] Danielyan L, Schafer R, von Ameln-Mayerhofer A, Bernhard F, Verleysdonk S, Buadze M, et al. Therapeutic efficacy of intranasally delivered mesenchymal stem cells in a rat model of Parkinson disease. Rejuvenation Res 2011;14(1):3–16.
[46] Andres RH, Choi R, Pendharkar AV, Gaeta X, Wang N, Nathan JK, et al. The CCR2/CCL2 interaction mediates the transendothelial recruitment of intravascularly delivered neural stem cells to the ischemic brain. Stroke 2011;42(10):2923–31.
[47] Hainsworth AH, Allan SM, Boltze J, Cunningham C, Farris C, Head E, et al. Translational models for vascular cognitive impairment: a review including larger species. BMC Med 2017;15(1):16.
[48] Glover JC, Aswendt M, Boulland JL, Lojk J, Stamenkovic S, Andjus P, et al. In vivo cell tracking using non-invasive imaging of iron oxide-based particles with particular relevance for stem cell-based treatments of neurological and cardiac disease. Mol Imaging Biol 2019.
[49] Mohseni M, Shojaei S, Mehravi B, Mohammadi E. Natural polymeric nanoparticles as a non-invasive probe for mesenchymal stem cell labelling. Artif Cells Nanomed Biotechnol 2020;48(1):770–6.
[50] Ashmore-Harris C, Iafrate M, Saleem A, Fruhwirth GO. Non-invasive reporter gene imaging of cell therapies, including T cells and stem cells. Mol Ther 2020;28(6):1392–416.